TITLE: Single-molecule sequencing of long DNA molecules allows high contiguity *de novo* genome assembly for the fungus fly, *Sciara coprophila*

AUTHORS: John M. Urban[1,2], Michael S. Foulk[1,3], Jacob E. Bliss[1], C. Michelle Coleman[4], Nanyan Lu[4], Reza Mazloom[4], Susan J. Brown[4], Allan C. Spradling[2] and Susan A. Gerbi[1]

[1]Brown University Division of Biology and Medicine, Department of Molecular Biology, Cell Biology and Biochemistry, Providence, Rhode Island 02912, USA

[2]Carnegie Institution for Science, Department of Embryology, 3520 San Martin Drive, Baltimore, Maryland 21218, USA

[3]Present Address: Mercyhurst University, Department of Biology, Erie, PA 16546, USA

[4]Kansas State University Division of Biology, KSU Bioinformatics Center, Ackert Hall, Manhattan, Kansas 66502, USA

CORRESPONDING AUTHORS:

Susan A. Gerbi

Brown University Division of Biology and Medicine

Sidney Frank Hall for Life Sciences

185 Meeting Street

Providence, RI 02912 USA

TEL: 401-863-2359/ FAX: 401-863-1201

E-mail: Susan_Gerbi@Brown.edu

John M. Urban

Carnegie Institution for Science

Department of Embryology

3520 San Martin Drive

Baltimore, Maryland 21218 USA

TEL: 410-246-3001

E-mail: jurban@carnegiescience.edu

RUNNING TITLE: The fungus fly genome

KEYWORDS: genome assembly, single molecule sequencing, long reads, optical maps, nanopore sequencing, DNA modifications, non-model organism, emerging model system, insect genomes, fungus fly *Sciara* (*Bradysia*) coprophila.

MANUSCRIPT TYPE: RESEARCH

DEDICATION: Dedicated to Ellen M. Rasch (January 31, 1927 – July 31, 2016), a leader in Feulgen-DNA cytophotometry who quantified the genome size of *Sciara coprophila*. Active in the American Society for Cell Biology (Council) and the Histochemical Society (Council, Secretary and Treasurer), she was a Fellow of the American Association for Advancement of Science and the Royal Microscopic Society.

ABSTRACT

The lower Dipteran fungus fly, *Sciara coprophila*, has many unique biological features. For example, *Sciara* undergoes paternal chromosome elimination and maternal X chromosome nondisjunction during spermatogenesis, paternal X elimination during embryogenesis, intrachromosomal DNA amplification of DNA puff loci during larval development, and germline-limited chromosome elimination from all somatic cells. Paternal chromosome elimination in *Sciara* was the first observation of imprinting, though the mechanism remains a mystery. Here, we present the first draft genome sequence for *Sciara coprophila* to take a large step forward in aiding these studies. We approached assembling the *Sciara* genome using multiple sequencing technologies: PacBio, Oxford Nanopore MinION, and Illumina. To find an optimal assembly using these datasets, we generated 44 Illumina assemblies using 7 short-read assemblers and 50 long-read assemblies of PacBio and MinION sequence data using 6 long-read assemblers. We ranked assemblies using a battery of reference-free metrics, and scaffolded a subset of the highest-ranking assemblies using BioNano Genomics optical maps. RNA-seq datasets from multiple life stages and both sexes facilitated genome annotation. Moreover, we anchored nearly half of the *Sciara* genome sequence into chromosomes. Finally, we used the signal level of both the PacBio and Oxford Nanopore data to explore the presence or absence of DNA modifications in the *Sciara* genome since DNA modifications may play a role in imprinting in *Sciara*, as they do in mammals. These data serve as the foundation for future research by the growing community studying the unique features of this emerging model system.

INTRODUCTION

The fungus gnat, *Sciara coprophila* (also known as *Bradysia coprophila*), is a Dipteran fly that is both an old and emerging model system rich with opportunities for studying fundamental biology, especially chromosomal biology due to its dynamic genome. In contrast to the rule that the amount of nuclear DNA is constant in all cells of an organism (Boivin et al. 1948), the nuclear DNA in *Sciara* cells exhibits copy number differences at the levels of loci, chromosomes, and the genome. Genomic copy numbers vary from canonical haploid and diploid tissues to the endocycling larval salivary glands that result in cells with over 8000 copies of each chromosome held closely together to form giant polytene chromosomes (Rasch 1970b). Locus-specific copy number regulation occurs at the “DNA puff” loci in polytene chromosomes where site-specific re-replication results in intrachromosomal DNA amplification (Rasch 1970a; Gerbi et al. 2002). Whole chromosome copy number gains and losses are seen in spermatogenesis, fertilization, in somatic cells of early embryos, and in the germ-line during development (Gerbi 1986).

The chromosome cycle of *Sciara* gives rise to numerous research opportunities not found in *Drosophila*, the standard Dipteran model organism. In *Sciara*, there are “L” chromosomes limited to the germ-line of both sexes (Gerbi 1986). Whereas oogenesis has orthodox chromosome movements, they are unusual in spermatogenesis leading to sperm cells that are haploid for each autosome, diploid for the X, and variable for the L with 0-4 copies. X diploidy in sperm is due to developmentally programmed X chromosome nondisjunction in male meiosis (Gerbi 1986). Fertilization ultimately produces zygotes and early embryos that are temporarily triploid for the X chromosome, and variable for the L. The fates of the X and L chromosomes in early embryonic nuclei are subsequently determined by whether a cell is somatic or germline, and by whether it is male or female. All L chromosomes are eliminated from somatic cell nuclei in early embryos. As part of the sex determination pathway, X diploidy is restored in female somatic cells (XX) by the elimination of one X, but the elimination of two X chromosomes in male somatic cells

(XO) leads to X haploidy (Gerbi 1986). Diploidy for the X and L is restored in the germline through elimination events later in development (Gerbi 1986).

The X chromosomes eliminated during early embryo development are always paternally derived. Moreover, all paternally derived chromosomes, except L, are eliminated in the first meiotic division of spermatogenesis in the only known case of a naturally occurring monopolar spindle (Gerbi 1986). The ability to differentiate between the maternal and paternal chromosomes gave rise to the term "imprinting" (Crouse 1960) and was the first description of this phenomenon in any system. L chromosomes apparently escape imprinting in *Sciara* as maternal and paternal copies are both eliminated from all nuclei destined to become somatic cells (Crouse et al. 1971), and they are not eliminated with the paternal cohort during male meiosis. The mechanism for imprinting in *Sciara* remains unknown. It is of interest to learn if DNA modifications occur in the *Sciara* genome, since imprinting in mammals utilizes DNA methylation (Li et al. 1993).

This black fungus gnat and its unusual chromosomal features are part of one of the most interesting yet little-studied groups of Dipteran flies, the suborder Nematocera. The group of Nematocerans contains agricultural pests as well as disease vectors, such as mosquitoes (Matthews et al 2018). Nematocera diverged from higher Dipteran flies, the suborder Brachycera that includes the fruit fly *Drosophila melanogaster*, ~200 million years ago (Wiegmann et al. 2011). *Bradysia (Sciara) coprophila* is classified as part of the infraorder Bibionomorpha in the Sciaroidea super family, which also comprises the family Cecidomyiidae (gall midges) and the Hessian fly in particular, a notorious wheat pest (Stuart et al 2012). Sciarid flies also include the Mycetophilidae, a fungus gnat family where members have been shown to withstand freezing and thawing (Sformo et al 2009). Indeed, we also have unpublished observations that *Sciara coprophila* embryos and larvae can be stored in the cold from a few months to over a year in a diapause-like state before returning to room temperature and resuming development. Despite flies making up at least 10%

of all metazoan diversity, there are only 157 Dipteran genomes described (i5k.github.io/arthropod_genomes_at_ncbi), most of which are highly fragmented assemblies, and the majority of which are from the higher Dipteran order and limited to only two suborders therein (Muscomorpha, Stratiomyomorpha). Thus, there is a real need for high quality genomes across the Dipteran tree, and particularly for the lower Dipteran suborder that includes *Sciara*.

The complete *Sciara* genome comprises three autosomes (chromosomes II, III and IV), an X chromosome, and the germ-line limited L chromosome (Figure 1; Gerbi 1986). L chromosomes are eliminated from nuclei destined to become somatic cells in the 5th or 6th nuclear division, ~3 hours after egg deposition (Gerbi 1986). *Sciara* lacks a Y chromosome, and sex is determined by whether or not the mother carries a variant of the X, called X', that has a long paracentric inversion. Females that are XX have only sons, whereas X'X females have only daughters. The XX or X'X genotype of adult females can be determined by phenotypic wing markers (Figure 1). The *Sciara* genome has ~38% GC content (Gerbi 1971) and is ~280 Mb in somatic cells and ~363 Mb in germ cells that contain L chromosomes (Rasch 2006) (Supplemental Table S1A-D).

There are many ways to assemble a genome, but no universal recipe of sequencing technologies, pre-assembly practices (e.g. quality filtering, error correction), assembly algorithms, parameter tuning, and post-assembly steps exists that guarantees the best assembly for a given genome. Therefore, to maximize contiguity and quality, we sequenced the *Sciara* genome with multiple technologies, including 100 bp Illumina paired-end reads, long reads from Pacific Biosciences (PacBio) (Eid et al. 2009) and the Oxford Nanopore MinION (Ip et al. 2015), and generated optical maps from the BioNano Genomics Irys platform (Lam et al. 2012). We produced assemblies using combinations of these technologies with multiple algorithms and ranked each using a battery of reference-free metrics. Highly contiguous assemblies that were most complete

in expected gene content and which were judged to be most consistent with our Illumina, PacBio, MinION, BioNano, and RNA-seq datasets were identified. These evaluations allowed us to monitor steps (e.g. polishing), to choose a few assemblies for BioNano scaffolding, and to make a final selection for the *Sciara* draft genome.

We report here the first draft genome assembly for *Sciara coprophila*, and its accompanying gene and repeat annotations. The *Sciara* genome sequence will be a valuable resource for future comparative genomics analyses, as one of the highest-quality Nematoceran genome sequences available, as the only sequenced member of the Sciaridae family, and due to its phylogenetic position at the gateway between lower and higher Dipterans. More than half of the *Sciara* genome is contained on contigs $\geq$1.9 Mb and scaffolds $\geq$6.8 Mb. This exceeds the contiguity of ~90% of all Dipteran genome assemblies (i5k.github.io/arthropod_genomes_at_ncbi). More specifically, the contig sizes in this release of the *Sciara* genome are longer than 42 of the 43 Nematoceran genome assemblies described, only outshined by the assembly for the mosquito, *Aedes aegypti* (Matthews et al 2018). The megabase-scale contigs and scaffolds will aid in efforts to improve the contiguity of more fragmented assemblies of related species by synteny. The genome annotation contains >97% of expected gene content. Up to 49% of the *Sciara* genome sequence was anchored into specific loci of chromosomes X, II, III, and IV; and 100% was classified as either X or autosomal, allowing an analysis of dosage compensation of the single male X. A *Rickettsia* genome was co-assembled with the *Sciara* genome, suggesting it may be an endosymbiont. The signal data from both PacBio and MinION both suggest the presence of DNA modifications in the *Sciara* genome. Finally, candidate L sequences were briefly explored. Sequencing, assembly, and annotation of the *Sciara* genome reported here serves as the foundation for future studies of the many unique features of this emerging model organism.

168 **Figure 1: Genome sequencing and assembly strategy for *Sciara coprophila***

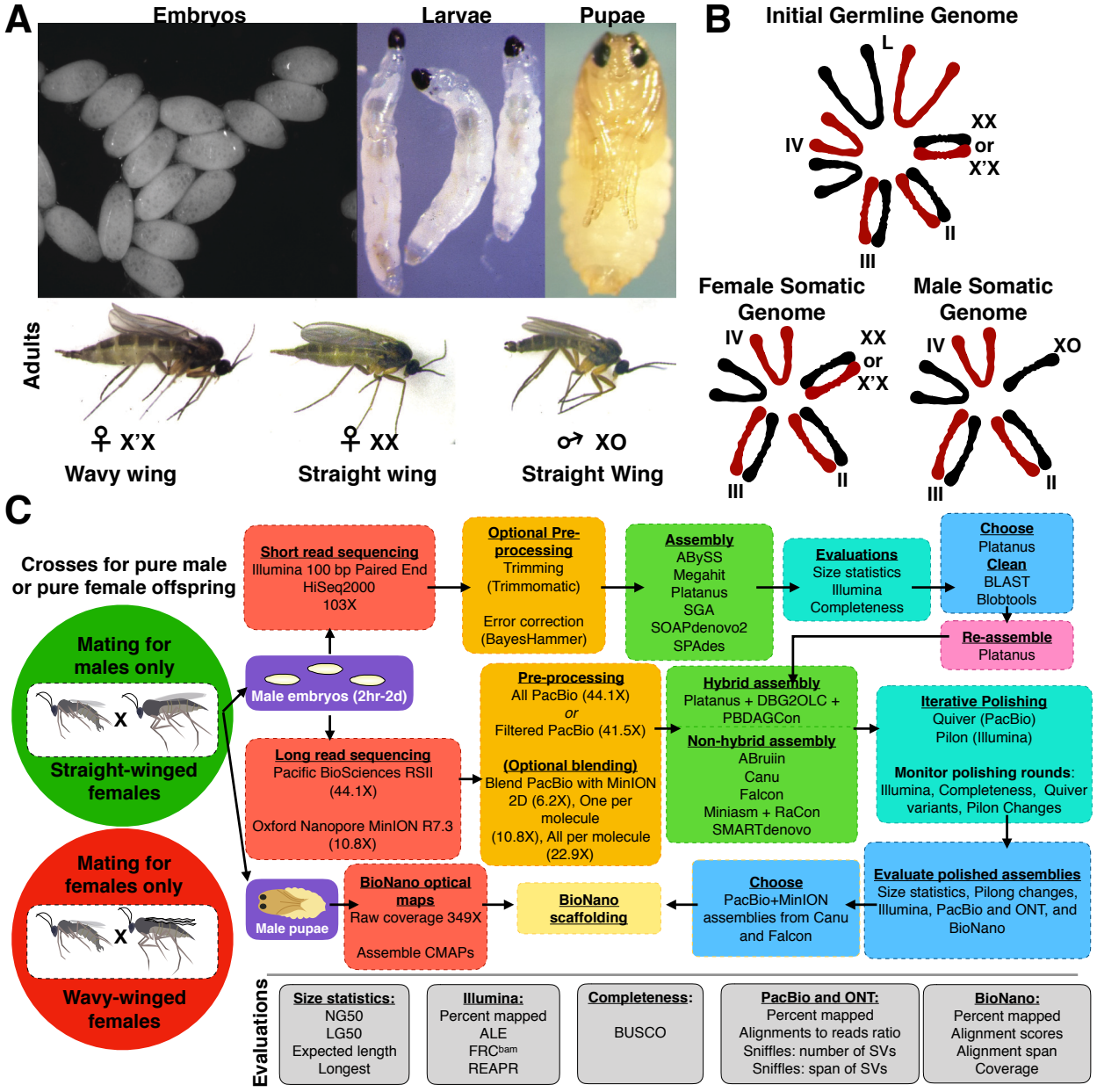

169
170 **Figure 1: Genome sequencing and assembly strategy for *Sciara coprophila***
171
172 **(A)** Images of different lifecycle stages of *Sciara coprophila*: embryos, larvae, pupae, and adults.
173 The adult figures show a male and the two different types of females that can be distinguished
174 based on the Wavy wing phenotype that marks the X' chromosome. **(B)** Examples of different
175 chromosome compositions in *Sciara* cells. We focused on the male somatic genome. Red
176 chromosomes are paternal, black are maternal. **(C)** The genome assembly and evaluation
177 workflow up until BioNano scaffolding. The workflow begins by highlighting that crosses can be
178 conducted to generate only male (green) or only female (red) offspring using the Wavy wing
179 phenotypic marker. We used only matings for males to obtain genomic DNA for sequencing,
180 illustrated by the arrows from the green circle that point to subsequent steps in the pipeline. Both
181 male (green) and female (red) offspring were used for transcriptomes.
182

RESULTS

Data collection

Using wing phenotypic markers, XX *Sciara* adult females were crossed with XO males to produce only male progeny (Figure 1). DNA isolated from purely male embryos was used for sequencing (Illumina, PacBio, MinION), thereby avoiding assembly complications from the heteromorphic X' chromosome found in female-producing females (Figure 1B), as well as minimizing possible complications from later life stages due to polytenization and contamination from the gut microbiome. Moreover, although early embryos were included to potentially capture sequences from chromosome L, the somatic genome is over-represented in these samples and we do not expect L sequences from the germline genome to be well-represented. Separate preparations of male embryo genomic DNA were made for 100 bp paired-end Illumina, and long-read PacBio and Oxford Nanopore MinION sequencing resulting in 103X, 50-55X, and 10-11X coverage, respectively (Table 1). We used male pupae to collect nearly 350X coverage from a third single molecule technology: optical maps from the BioNano Genomics (BNG) Irys (Lam et al. 2012) (Table 1). Finally, to facilitate gene annotation, we acquired sex- and stage-specific 100 bp paired-end RNA-seq datasets from whole embryos, larvae, pupae, and adults using the appropriate crosses for only males (XX x XO) or only females (X'X x XO) (Supplemental Table S2).

201 **Table 1: Genome sequencing datasets for *Sciara coprophila***

	Illumina HiSeq 2000	PacBio RSII	Oxford Nanopore MinION Mkl	BioNano Genomics Irys
Source	Male Embryos	Male Embryos	Male Embryos*	Male pupae
Library	Paired-End*	SMRTBell	MAP002-006 (2D)	IrysPrep
Details	-	P5-C3	Pores R7.3-R7.3 70bps 6mer	BssSI
Read Length N50 (kb)	0.1	9.681	9.934	132.613
Mean Read Length (kb)	0.1	6.607	5.883	62.531
Count	301,513,554	1,949,427	532,714	1,628,681
Span (Gb)	30.15	12.88	3.15	101.84
Coverage >0 kb	103.26	44.11	10.77	348.78
>20 kb	0	1.28	2.91	330.22
>30 kb	0	0.01	1.72	323.31
>50 kb	0	0	0.71	303.02
>100 kb	0	0	0.28	226.1
>150 kb	0	0	0.2	148.5

202 *A minority of the MinION data came from male adults (see Methods).

Short-read assemblies

Using the Illumina dataset, both with and without quality filtering and/or error-correction steps, we generated 44 assemblies using 7 popular short-read genome assemblers (Figures 1C and 2A). The assemblies ranged from ~226-348 Mb in size (Supplemental Table S3), with a mean assembly size of ~280 Mb, exactly the expected somatic genome size. Evaluating these assemblies with several reference-free evaluation tools (see Methods) allowed us to determine the highest quality assemblies (Figures 1C, 2A-D, Supplemental Figure S1). Rankings from these metrics were generally correlated with each other (Figure 2A, Supplemental Figure S2A). Platanus and ABySS assemblies most consistently returned the best rankings across metrics with Platanus assemblies having higher mean ranks overall (Figure 2A and Supplemental Figure S1). All Illumina assemblies did moderately well in terms of gene content, most containing between 80-85% of the expected Arthropod BUSCOs (Figure 2B). Nonetheless, all of the Illumina assemblies were highly fragmented, containing up to hundreds of thousands of contigs mostly less than 1 kb in length. The NG50 values ranged from 2.5-7.3 kb (Figure 2C, Supplemental Table S3). Although some scaffolds in the assemblies reached up to the Mb range, they were all bacterial, a common observation for assemblies from whole animals (Supplemental Figure S3). Of recognizable bacterial sequence, at the genus level, ~90% was characterized as *Delftia* and ~5% as *Rickettsia*. Amongst all Illumina assemblies, the longest scaffolds of apparent insect origin were 50-60 kb. Filtering for bacterial contamination and re-assembling with the filtered data did not improve the contiguity (Supplemental Table S3). Although short-read-only assemblies were not pursued further, the highest quality Platanus assembly was used in hybrid assemblies with long reads, and the high accuracy Illumina short reads were useful for polishing long-read assemblies.

Figure 2: Assembly evaluations

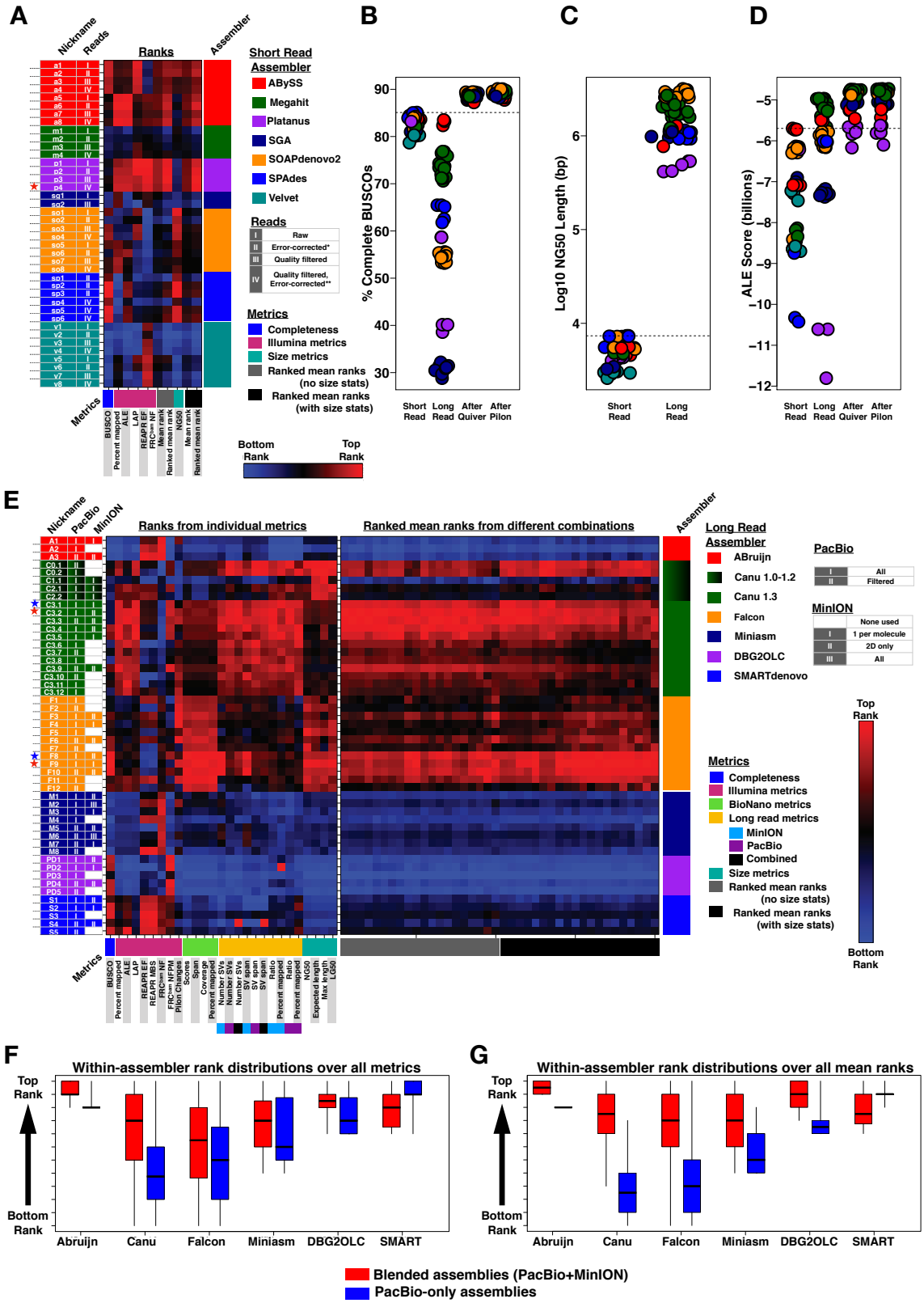

Figure 2: Assembly evaluations. (A) Rank matrix for 40 Illumina assemblies. Each column corresponds to a metric. Each row corresponds to an assembly. The columns and rows are organized by metric class and assembler, respectively. Multiple assemblies were generated for each assembler differing by the input reads, parameters used, or both. Assembly nicknames allow finding the assemblies in supplementary tables and methods. Assembly ranks for each metric span from lowest (blue) to highest (red) in each column. Assemblies (rows) that do well across the metrics tend to be mostly shades of red. The red star marks the Platanus assembly that performed best overall and was used as the input for hybrid assemblies. **(B-D)** Use the short-read assembly color scheme from (A) and the long-read color scheme from (E) to visualize **(B)** percent of complete BUSCOs found, **(C)** Log10 NG50 lengths, and **(D)** ALE scores for short-read and long-read assemblies. B and D show the long-read scores before and after polishing steps. The dotted lines in (C) represent the maximum NG50 from short-read assemblies. **(E)** Rank matrix for 50 long-read assemblies organized as described in A. Red and blue stars mark assemblies brought into BioNano scaffolding. Red stars represent the scaffolded assemblies that were chosen after BioNano scaffolding. **(F-G)** Box and whisker plots of within-assembler rank distributions comparing blended (red) to PacBio-only (blue) inputs to each assembler. The boxplots are not comparable between assemblers. The boxes show the 25^{th}-75^{th} percentile, the black line is the median, and the whiskers span the range (min to max). Assemblies from a given assembler were ranked either using (F) all individual metrics from E or (G) all ranked mean ranks from different combinations of metric ranks from E. The ranks were then partitioned into those from blended versus PacBio-only assemblies. In both cases (F-G), blended assemblies from all assemblers except SMARTdenovo had significantly higher ranks by Wilcoxon Rank Sum Test than PacBio-only assemblies from the same assembler.

Long-read datasets and assemblies

A route to obtaining more contiguous assemblies is incorporating data from single molecule, long-read technologies, such as Single Molecule Real Time (SMRT) sequencing from Pacific Biosciences (PacBio) and nanopore sequencing with the MinION from Oxford Nanopore Technologies (ONT). These technologies are more error-prone than Illumina, but the errors are approximately randomly distributed allowing high quality consensus sequences with enough coverage (Eid et al. 2009; Ip et al. 2015; Loman et al. 2015). Both long-read technologies produced read lengths that exceeded the scaffold lengths in the Illumina short-read assemblies, particularly MinION reads obtained using our modified protocols (Supplemental Figure S4; Urban et al 2015). Thus, even before attempting to assemble the long reads, we had a richer source of long-distance information than the short-read assemblies provided.

The majority of long-read coverage (50-55X total) was from PacBio (44.1X; Table 1; Supplemental Figure S4), and we were able to produce high quality assemblies using PacBio reads alone. However, despite having four times lower coverage, the MinION data (10.77X) had in excess of two times more coverage from molecules greater than 20 kb and over a hundred times more coverage from molecules exceeding 30 kb than the PacBio data (Table 1). Over 10% of the MinION data was from molecules that surpassed the longest PacBio read length of 36 kb, approximately a third of which came from high quality 2D reads (Table 1, Supplemental Figure S4). Validation of the MinION reads on assemblies generated from the PacBio data alone showed many high quality 1D and 2D reads (Supplemental Figure S5). These included hundreds of 2D reads exceeding 50 kb and several >100 kb that aligned across their full lengths with percent identities up to 94.6%. One notable 131 kb MinION 2D read aligned with 91.1% accuracy to the PacBio data. This gave us an opportunity to test whether even a small amount of ultra-long MinION reads could improve upon the PacBio assemblies. Therefore, we also generated assemblies from a blend of both single-molecule technologies, referred to here as “blended

277 assemblies" to differentiate them from "hybrid assemblies" that refers to combining short-read and
278 long-read technologies (Figure 1C).
279
280 In total, we generated 50 assemblies using long reads (Figure 1C), including hybrid
281 assemblies that started from Illumina contigs. We evaluated the long-read assemblies with the
282 same metrics used to rank the short-read assemblies (Figure 2 B-D, Supplemental Figure S1).
283 Before polishing, ABruijn and Canu assemblies rose highest in most rankings (Figure 2 B-D,
284 Supplemental Figure S1), perhaps because these assemblers had the best consensus sequence
285 modules. Even before polishing, most long-read assemblies outperformed short-read assemblies
286 for percent error-free bases (REAPR) and had comparable or better scores in other metrics (e.g.
287 LAP, ALE, FRC). However, most underperformed in terms of gene content with fewer than 80%
288 BUSCOs detected (Figure 2 B-D, Supplemental Figure S1).
289
290 **Long-read assembly polishing and monitoring**:
291 To ensure that the assembly evaluations primarily reflected the structural integrity of each
292 assembly rather than differences in consensus quality, we employed extensive post-assembly
293 polishing using Quiver (Chin et al 2013) and Pilon (Walker et al 2014) (Figure 1C). We monitored
294 the outputs from each round of polishing using the metrics discussed above as well as the number
295 of variants detected and changes made by the polishing algorithms (Figure 1C). The assemblies
296 started out with up to millions of Quiver variants and converged to just a few thousand, and
297 evaluations improved across Quiver rounds, with the biggest impact occurring in the first round
298 (Supplemental Figure S6). After Quiver polishing, Canu assemblies continued to take many of
299 the highest ranks whereas ABruijn assemblies lost their lead (Figure 2 B-D, Supplemental Figure
300 S1). Quiver polishing also closed the gaps between the highest and lowest scoring assemblies in
301 each metric. For example, whereas the percent of BUSCOs detected ranged from 30-83% prior
302 to Quiver polishing, ~90% were detected in all assemblies after (Figure 2B). Moreover, all polished

long-read assemblies outperformed the best scoring short-read assemblies in each metric, with the exception of the hybrid assemblies that still underperformed on the ALE metric (Figure 2D). The Illumina-based metrics favored non-hybrid long-read assemblies over both the short-read and the hybrid assemblies that were constructed from the same Illumina data. This speaks to the structural and consensus quality of the contig sequences derived from long reads alone (Figure 2D, Supplemental Figure S1; "After Quiver"). Nevertheless, Illumina-polishing with Pilon improved the consensus further, fixing 19.2-25.8 thousand base and small indel errors (~60-90 errors/Mb) in the first round, and 0.9-2.4 thousand (~3-8 errors/Mb) in the second. The small number of corrections introduced in the final round indicates long stretches (hundreds of kb) of high-quality consensus sequences between any remaining errors in the final assemblies. Accordingly, Pilon tended to improve evaluations modestly over what Quiver had already accomplished (Figure 2B, 2D, Supplemental Figure S1; "After Pilon"). For example, it resulted in detecting up to an additional 1.05% of BUSCOs (0.63% on average).

Selecting assemblies for BioNano scaffolding:

After polishing, the number of variants or genes detected and other metrics that reflect consensus sequence quality converged to similar scores across assemblies. This allowed us to focus on the size and long-range integrity of contigs when making selections for scaffolding with optical maps. We used an expanded battery of reference-free metrics to guide our choice of which assemblies to scaffold (Figures 1C and 2E). The additional metrics were based on long reads and optical maps (see Methods). There was general agreement on assembly rankings among metrics from the four orthogonal technologies (Supplemental Figure S2B).

Long-read assembly sizes ranged from 281.5-306.6 Mb (Supplemental Table S4), close to the expected *Sciara* male somatic genome size of 280 Mb. All long-read assemblers produced assemblies that were orders of magnitude more contiguous than short-read assemblies. NG50s

were typically in the Mb range and all exceeded 100 kb (Figure 2C, Supplemental Figure S1F, Supplemental Table S4). For all size metrics, assemblies from Canu and Falcon ranked highest (Figure 2C, 2E), with the largest NG50s of 3.08 Mb and 3.17 Mb, respectively (Figure 2C "Long Read", Supplemental Table S4). Canu and Falcon assemblies also had the lowest LG50s containing 50% of the expected genome size on just 21 and 23 contigs, respectively (Supplemental Figure S1F, Supplemental Table S4). The highest normalized expected contig sizes (Salzberg et al. 2012) for assemblies from Canu and Falcon exceeded 5 Mb and the longest contigs from each exceeded 20 Mb (Supplemental Figure S1F, Supplemental Table S4).

Longer contigs can simply be a consequence of more aggressively joining reads at the cost of more misjoins. Therefore, we interrogated whether Canu and Falcon assemblies, which had the longest contigs, suffered from higher error rates. However, in direct opposition, Canu and Falcon assemblies were consistent rank leaders in our battery of evaluations (Figure 2E). Canu assemblies led most Illumina-based and long-read metrics. Falcon assemblies led BioNano metrics and gene content (Figure 2E; Supplemental Figure S1), although differences in gene content were negligible (Figure 2B). Canu and Falcon assembles had fewer putative mis-assemblies than others as proxied, for example, by long-read detection of structural variants (Supplemental Figure S7J). They also had apparently higher long-range integrity according to BioNano map alignments, which spanned a range of 237-252 Mb in Falcon and Canu assemblies, but only 181-230 Mb in others (Supplemental Figure S7H, S7J, S7L). In sum, Canu and Falcon assemblies had longer contigs and ranked higher than other assemblies in most metrics (Figure 2E), the latter arguing against more misjoins.

To select a final subset of assemblies for BioNano hybrid scaffolding, we sorted the assemblies by taking mean ranks across 40 combinations of the 27 metrics (Figure 2E). In general, blended assemblies tended to rank higher than their PacBio-only counterparts for 5 of

355 the 6 long-read assemblers, although this often reflected modest improvements in the actual
356 scores. The largest variation amongst scores tended to reflect the assembler used (Figure 2 F-
357 G, Supplemental Figure S7). Blended assemblies from Canu and Falcon were the clear rank
358 leaders again in this final analysis (Figure 2 E-G), and two assemblies from each were chosen for
359 BioNano hybrid scaffolding. The chosen assemblies were constructed from all 44X PacBio data
360 and either only 2D MinION reads (6.2X) or 1D and 2D reads (10.8X).
361

362 **FIGURE 3: Post-assembly work flow:**

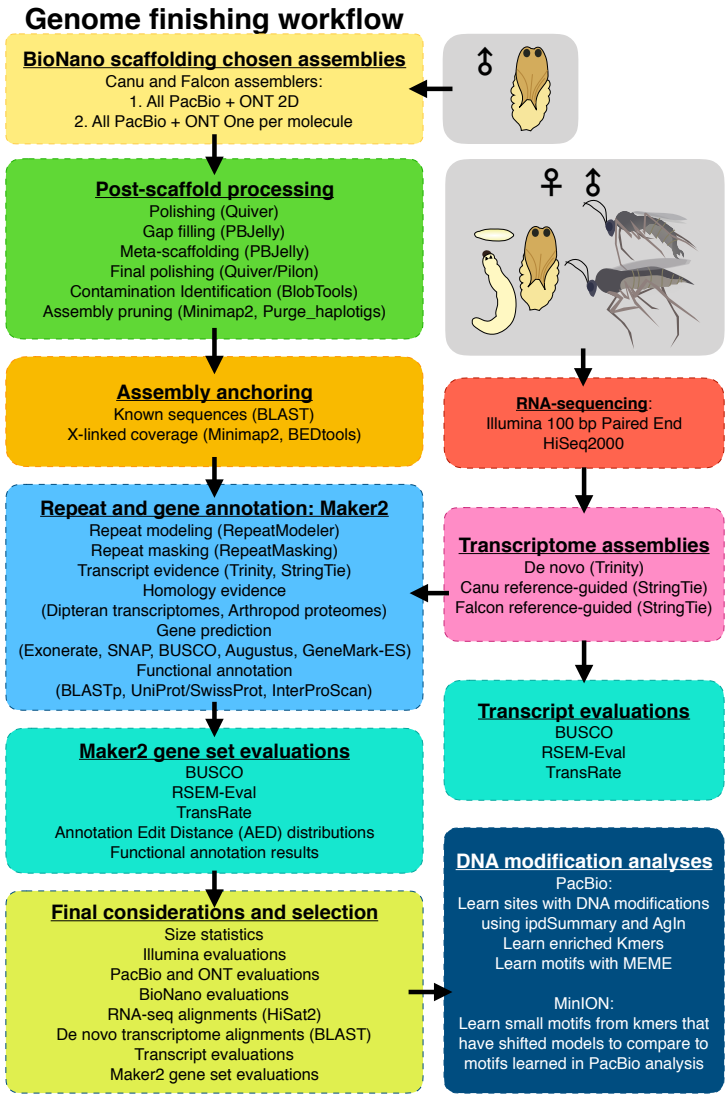

363

364 **FIGURE 3: Post-assembly work flow:**

365 Workflow starting after selecting assemblies for BioNano scaffolding. Chosen assemblies were
366 scaffolded, polished, gap-filled, filtered for contamination, anchored into chromosomes by
367 sequences with known chromosomal addresses, and anchored to the X or autosomes by haploid
368 or diploid coverage. Repeats were characterized and RNA-seq was used to facilitate
369 transcriptome assembly and gene annotation. The single-molecule datasets were re-used to
370 investigate DNA modifications.

371 **Scaffolding with optical maps**

372 We obtained BioNano Irys optical map data from male pupae (Figure 3, Table 1). The raw
373 molecule N50 was 214.1 kb for molecules >150 kb. The genomic consensus maps (CMAPs)
374 produced from them had a map N50 of 712 kb and a cumulative length of 325.5 Mb. Thus, the
375 genome length estimated from the CMAPs was between the expected sizes of the somatic and
376 germline genomes. The CMAPs spanned 266-278 Mb of the Canu and Falcon contigs. The
377 CMAPs and sequence assemblies were used to produce the hybrid scaffold maps. Both the
378 CMAPs and sequence contigs had similar spans across the hybrid scaffold maps of approximately
379 275-280 Mb. We found that the hybrid scaffolds derived from both Canu assemblies and from
380 both Falcon assemblies were nearly identical as determined by evaluation metrics and whole
381 genome alignments (Supplemental Figures S8-S9, Supplemental Table S5). Therefore, we chose
382 the single scaffold set from each pair that was evaluated to be slightly better, hereafter referred
383 to as “Canu” and “Falcon”. Hybrid scaffolding approximately tripled the contiguity of the
384 assemblies (Figure 4A, Supplementary Tables S6, S7). Throughout the following text, Canu
385 assembly statistics will be described with corresponding Falcon statistics in parentheses. The
386 total numbers of sequences in the Canu (Falcon) assembly decreased from 1044 to 857 (713 to
387 608) while increasing the NG50 of 2.3 Mb to 6.7 Mb (3.5 Mb to 10 Mb). The assembly size also
388 increased from 302 Mb to 311 Mb (296 Mb to 303 Mb) (Figure 4A-C). The Canu (Falcon) scaffolds
389 had 187 (105) gaps summing to 8.7 Mb (6.7 Mb) with a maximum gap size of 677 kb (965 kb)
390 and median of 20.8 kb (30.5 kb) (Supplemental Table S8).
391
392 We next iteratively filled and polished the gaps using PBJelly (English et al. 2012) and
393 Quiver, respectively. In the Canu (Falcon) scaffolds, 31 (14) gaps were completely closed and
394 over 972 kb (1.06 Mb) of gap sequence was filled in (Figure 4C, Supplemental Table S8). In the
395 final round of gap filling, we allowed PBJelly to “meta-scaffold” the hybrid scaffolds using
396 connections from long-read alignments. This decreased the total number of sequences in Canu

(Falcon) from 857 to 769 (608 to 565) while increasing the NG50 of 6.7 Mb to 8.3 Mb (10.0 Mb to 10.5 Mb) and the assembly size from 311 Mb to 312 Mb (303 Mb to 304 Mb) (Figure 4A, Supplemental Table S6, S7). We used both Quiver and Pilon to correct errors in the gap-filled meta-scaffolds. In the final round, Pilon made only 18-27 changes to the consensus sequences, translating to 1 change per 16.9 Mb and 11 Mb of non-gap sequence for Canu and Falcon, respectively.

403 **Figure 4: Assembly scaffolding and anchoring**

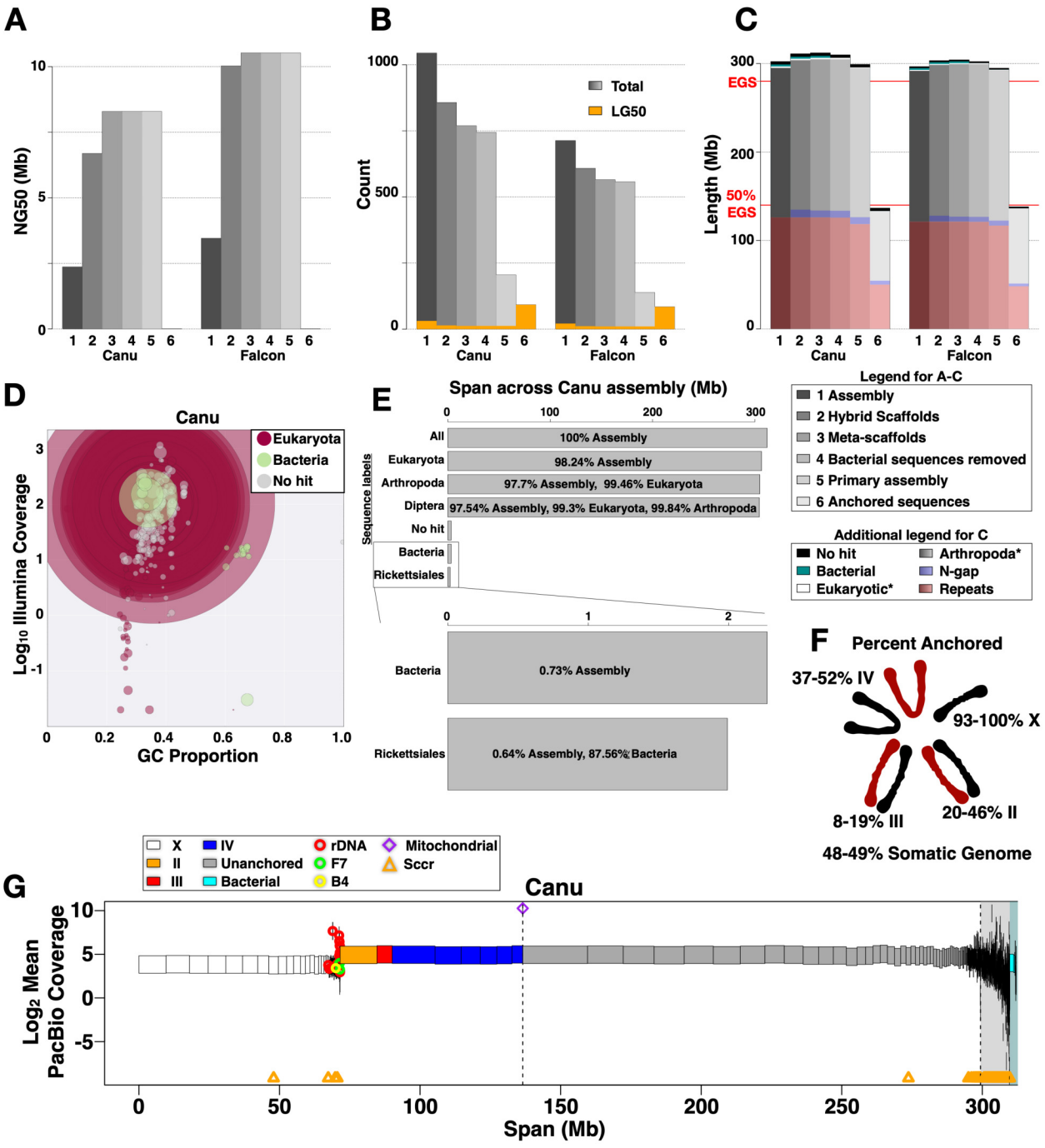

404

405

Figure 4: Assembly scaffolding and anchoring

(A) NG50 of the assembly at different stages 1-6 as defined in "Legend for A-C" within the figure. **(B)** Number of sequences in the assembly at different stages 1-6 as in A. The orange portions are LG50 counts, or the number of the longest sequences in each set needed to reach 50% of the estimated genome size (EGS = 280 Mb) for the somatic genome. **(C)** The total length of the assembly at different stages 1-6 as in A. The "Additional legend for C" defines colored portions of the bars. *The length of the Eukayotic and Arthropod labeled sequences includes everything up through that color. **(D)** Log10 Illumina coverage versus GC content over the Canu assembly (similar results for Falcon), colored by taxonomy information, and with circle sizes proportional to the contig sizes they represent. **(E)** The proportion of the assembly taxonomically labeled as Eukaryotic, Arthropoda, Diptera, Bacteria, and Rickettsiales. **(F)** The percentage of the expected genome size and chromosome sizes that has been anchored. Ranges represent range in Canu and Falcon assemblies. Colors as in Figure 1. **(G)** The Canu assembly with scaffolds drawn as rectangles corresponding to their lengths, colored according to the chromosome they were anchored into (or unanchored), and at their mean coverage from PacBio reads, the dataset used to determine X-linked sequences by haploid level coverage. The white background highlights sequences in the primary assembly whereas the grey and cyan backgrounds are set behind associated and bacterial sequences, respectively. All sequences to the left of the first vertical dashed line are anchored.

425 **Assembly cleaning**

426 BlobTools (Laetsch and Blaxter 2017) was used to identify contaminating contigs in the
427 final scaffolds (Figure 4C-E, Supplemental Figure S10, S11). *Sciara* male embryo coverage from
428 Illumina, PacBio, and the MinION all gave similar results (Supplemental Figure S10). The vast
429 majority of the final Canu and Falcon scaffolds (≥97.7% of the total sequence length) was
430 identified as Arthopoda, >99% of which was also Dipteran (Figure 4C, 4E, Supplemental Figure
431 S11). Canu and Falcon had 25 and 8 bacterial contigs respectively, with total lengths of 2.0-2.3
432 Mb (<1% of the total sequence length) and bacterial contig N50s of 1.0-1.3 Mb (Figure 4C, 4D,
433 4E, 4G; Supplemental Figure S11, Supplemental Table S9). There were no BioNano optical map
434 alignments over the bacterial contigs, and accordingly there were no bacterial contigs attached to
435 or found in any of the final Arthropod-associated scaffolds. Removing bacterial contigs only
436 marginally affected contig size statistics of the *Sciara* assemblies (Figure 4G; Supplemental
437 Tables S6, S7).
438
439 No bacterial contigs were labeled as Delftia in the long-read assemblies despite it being
440 the major bacterial representation in short-read assemblies. The majority of the bacterial
441 sequence (87-96%) in the Canu and Falcon scaffolds was labeled as Rickettsiales (Figure 4D-E,
442 Supplemental Figure S11), nearly all of which was associated with *Rickettsia prowazekii* (88.5-
443 90.1%) and *Rickettsia peacockii* (9.9-10.8%). Given that the published genome sizes for these
444 *Rickettsia* species range from ~1.1-1.3 Mb (Andersson et al. 1998; Felsheim et al. 2009), it is
445 possible that a complete *Rickettsia* genome sequence was co-assembled. The genus *Rickettsia*
446 includes obligate intracellular bacteria that may be the closest extant relatives to the ancestor of
447 the mitochondrial endosymbiont (Andersson et al. 1998). *Rickettsia* is closely related to
448 *Wolbachia* that is found in many strains of *Drosophila melanogaster* (Clark et al. 2005). The
449 *Rickettsia* or *Rickettsia*-like species in our *Sciara* datasets may be an important part of *Sciara*
450 biology. Interestingly, in the Illumina, PacBio, and MinION datasets, the *Rickettsia* genome has

nearly the same coverage as the *Sciara* genome (Figure 4D, 4G, Supplemental Figure S10). This indicates that there is approximately one *Rickettsia* genome per haploid *Sciara* genome or two *Rickettsia* for each diploid *Sciara* cell in male embryos on average. The current evidence can only suggest that this correspondence is coincidental. Despite high Rickettsia coverage in embryos, there were no *Rickettsia* optical maps from pupae. This may reflect the DNA plug isolation procedure used and/or a far lower abundance of *Rickettsia* in pupal cells or its restriction to a small subset of cells.

After removing bacterial sequences, each assembly was partitioned into “primary” and “associated” sequences. Primary sequences represent one haplotype of the genome whereas associated sequences consist of short redundant contigs called haplotigs that represent other haplotypes of specific loci (Figure 4G). The Canu (Falcon) assembly contained 744 (557) sequences of which 205 (138) were primary and 539 (419) were associated, giving a primary assembly size of ~299 Mb (~295 Mb) with ~13 Mb (9.4 Mb) of associated sequences (Figure 4A-C, Supplemental Tables S6, S7). The difference of ~4 Mb between the Canu and Falcon primary assembly sizes is in part owed to Canu having ~2.2 Mb more gap length than Falcon. Given that the associated sequences are generally short (~23 kb on average), computing size statistics on the primary assembly has relatively large effects on the mean and median contig sizes (Supplemental Tables S6, S7). For example, the mean scaffold size in Canu (Falcon) increased from ~416 kb to 1.5 Mb (542 kb to 2.1 Mb).

471 **Table 2: Anchoring into chromosomes using previously known sequences**

Sequence	Location	Canu contig size	Falcon contig size	Reference
DNA puff II/9A	Chr II locus 9A	13.1 Mb	28.5 Mb	DiBartolomeis and Gerbi 1989; Bienz-Tadmor et al. 1991; Urnov et al 2002; Foulk et al. 2006
RNA Puff III/9B	Chr III locus 9B	5.4 Mb	12.5 Mb	Wu et al 1993; Foulk et al. 2006
Ecdysone receptor	Chr IV locus 12A	3.8 Mb	9.6 Mb*	Foulk et al 2013
Ultraspiracle	Chr IV locus 10A	9.3 Mb	5.5 Mb	Foulk et al 2013
Hsp70	Chr IV locus 4A or 12C	5.4 Mb	13 Mb	Mok et al. 2000
Hsp70	Chr IV locus 4A or 12C	6.8 Mb	2.6 Mb	Mok et al. 2000
ScoHet1	Chr IV locus 5A	15.2 Mb	(9.6 Mb)*	Greciano et al. 2009
ScoHet2	Chr IV locus 12C-13A	5.9 Mb	4 Mb	Greciano et al. 2009
rDNA	End of Chr X	5 primary contigs and 11 associated contigs (Σ 1.3 Mb)	2 primary contigs and 41 associated contigs (Σ 1.7 Mb)	Pardue et al. 1970; Gerbi 1971; Crouse et al. 1977; Kerrebrock et al. 1989
Microclone B4	End of Chr X	69.8 kb	59 kb	Escribá et al. 2011
Microclone F7	Near centromere of Chr X**, non-centromeric Chr IV, L chromosomes	3 associated contigs (Σ 66.8 kb)	1 primary and 1 associated contig (Σ 161.6 kb)	Escribá et al. 2011
Microclone G2 (Sccr)	Centromeres of all chromosomes	20 primary and 85 associated contigs (Σ 1.3 Mb)	6 primary and 42 associated contigs (Σ 604 kb)	Escribá et al. 2011

472 *Ecdysone receptor (EcR) and ScoHet1 identified the same 9.6 Mb contig in Falcon. The locus
473 inconsistency may represent a misassembly in Falcon or misannotation from Greciano et al
474 (2009). Nevertheless, both EcR and ScoHet1 results agree it is from chr IV.
475 ** Coverage analyses confirm contigs with F7 as chromosome X sequence.

476 **Assembly anchoring**

477 We used previously known sequences with associated *in situ* hybridization results from
478 polytene chromosomes to anchor some of the scaffolds into chromosomes (Table 2). The results
479 span all 3 autosomes and the X chromosome. We anchored 7-8 primary autosome-linked contigs
480 from each assembly that sum to 64.9-75.6 Mb, or ~23-27% of the expected somatic genome size
481 and 28-33% of the expected autosomal sequence length. Given the number of regions
482 determined for each chromosome from polytene banding patterns (Gabrusewycz-Garcia 1964),
483 we expect chromosomes II, III, and IV to be approximately 62-66 Mb, 66-71 Mb, and 88-94 Mb,
484 respectively (Supplementary Table S1E). Therefore, across both assemblies we expect to have
485 anchored 20-46% of II, 8-19% of III, and 37-52% of IV. Since it is possible to transfer anchoring
486 information from one assembly to the other, the overall anchoring percentages for both
487 assemblies are essentially the higher end of each range above. We also anchored between 1-2
488 Mb of X-linked contigs using repetitive sequences specific to the X (Table 2, e.g. rDNA). In
489 addition to chromosome-specific sequences, “Sccr” (*Sciara* centromere consensus sequence)
490 that hybridized to the centromeres of all *Sciara* chromosomes (Escribá et al. 2011) mapped to 48-
491 105 contigs, the majority of which were not primary sequences (Table 2).
492
493 The majority of genomic DNA sequenced from male embryos came from somatic cells that
494 are haploid for the X and diploid for all autosomes. Therefore, X-linked contigs could be defined
495 as primary contigs with haploid level coverage across 80% or more of their lengths. The Canu
496 (Falcon) assembly contained 69 (36) contigs called as X that summed to 71 Mb (62 Mb) with the
497 longest X-linked contig reaching 9.68 Mb (12 Mb) and an X-linked contig N50 of 5.95 Mb (7.3
498 Mb). In both assemblies, contigs containing the X-hybridized repetitive sequences (Table 2: rDNA,
499 B4) were called as X as expected (Figure 4G, Supplemental Figure S11C). Upon closer
500 inspection, contigs with rDNA not called as X had haploid level coverage regions interrupted by
501 regions of unusually high coverage over collapsed rDNA repeats, and were therefore consistent

with being X-linked sequences as well. We also found X-linked contigs that contained the F7 repeat sequence known to be on X, IV, and L (Escribá et al. 2011) (Figure 4G, Supplemental Figure S11C). The X chromosome is estimated to be ~50 Mb based on DNA-Feulgen cytophotometry or ~62 Mb based on the number of polytene bands (Rasch 2006; Gabrusewycz-Garcia 1964; Supplementary Table S1 A-E). Therefore, >93% of the X chromosome sequence could be anchored. In total, at least 136.6-138.0 Mb of *Sciara* sequence, or ~49% of the expected somatic genome size, was anchored into specific chromosomes with 100% of the assembly characterized as either X or autosomal from the coverage analysis.

510 **Figure 5: Repeats and genes in the chosen assembly**

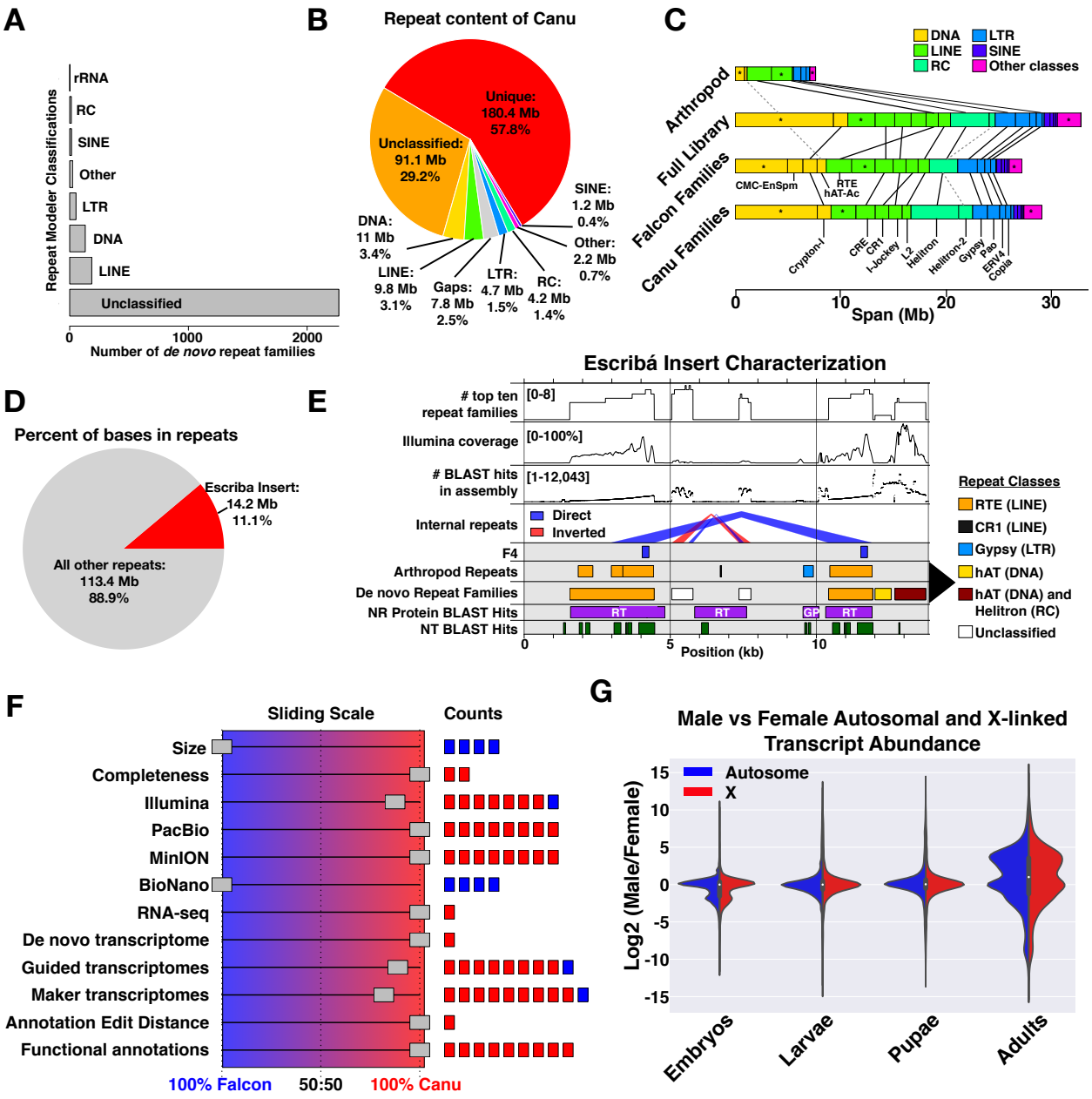

511

512 **Figure 5: Repeats and genes in the chosen assembly**

513 **(A)** Number of *de novo* repeat families trained on Canu with each classification. **(B)** Pie chart

514 partition of the Canu assembly into the major repeat categories. Note that the “DNA” label used

515 by RepeatMasker refers to DNA transposons. **(C)** The major sub-classes of repeats in each

516 repeat class in the Canu assembly, showing the results when using different repeat libraries for

masking. **(D)** Pie chart representing the number of bases masked by the Escribá insert (Escribá et al. 2011) alone compared to all masked bases. **(E)** Characterization of the Escribá insert, highlighting major repeats in the *Sciara* genome. Black arrowhead on right side pointing to repeat classes legend corresponds only to the two repeat family rows. RT = reverse transcriptase. GP = gag-pol. **(F)** The ranking results of the final two assemblies demonstrating how many metrics in each category for which each assembler scored better. **(G)** Split violin plots showing the log2 of the male to female ratio of transcript abundance for the X (red) and autosomes (blue) across multiple life stages.

525 **Repeats in the *Sciara* genome**

526 To learn more about the repeat content of the *Sciara* genome and to facilitate repeat masking,
527 *de novo* repeat families were created from both the Canu and Falcon assemblies using
528 RepeatModeler (Smit and Hubley 2008). There were close to 2700 repeat families in each library
529 of which 15-19 were classified as SINEs, 160-186 as LINEs, 48-53 as LTR, 130-131 as DNA
530 elements, and 43-50 as other repeat classes (Figure 5A, Supplemental Figure S11D,
531 Supplemental Tables S10, S11). The majority of repeats in each library were unclassified. For
532 repeat masking, the *de novo* repeat libraries were combined with the few previously known repeat
533 sequences (see Methods) as well as repeats from across Arthropods. Using this comprehensive
534 repeat library, RepeatMasker (Smit et al. 2013) classified ~121-126 MB or 39-41% of the Canu
535 and Falcon assemblies as repeats (Figure 5B, Supplemental Figure S11E, Supplemental Tables
536 S12, S13). Assuming that scaffold gaps also correspond to repeats leaves ~180 Mb of unique
537 sequence (~58%) in the Canu assembly (Figure 5B). The majority (76.6-76.9%) of repeats were
538 unclassified and spanned 93.3-96.7 Mb (Figure 5B) whereas SINE, LINE, LTR, RC, and DNA
539 elements each constitute 0.4-3.4% of the assemblies (Figure 5B). DNA elements made up the
540 largest class in terms of total span and Crypton-I was the largest sub-class therein (Figure 5C).
541 However, Helitron elements from the RC class were the largest sub-class in the assembly overall
542 (Figure 5C). Simple repeats made up ~1% of the assemblies (Supplemental Table S12). Similar
543 results were obtained when repeat masking with only the *de novo* repeat libraries (Figure 5C).
544 However, using only known arthropod repeats found fewer, had a higher composition of LINE
545 elements, and found the RTE sub-class therein to be the most abundant sub-class in the
546 assembly (Figure 5C).
547
548 Previously, Escribá et al. (2011) published a 13.8 kb lambda phage insert sequence that
549 contains two copies of the non-LTR retrotransposon named ScRTE. A corresponding probe (F4)
550 predominantly labeled pericentromeric regions of all *Sciara* chromosomes by FISH (Escribá et al.

2011). We found that the 13.8 kb Escribá insert contains some of the most abundant sequences in the *Sciara* genome, although there was only one full-length copy of the lambda insert in each assembly presumably from the locus that was originally cloned (Supplemental Figure S12). Otherwise, pieces of the insert were scattered across the assembly corresponding to nearly 60,000 alignments spanning ~14.2 Mb, or ~11% of bases labeled as repeats (Figure 5D-E). Of the top ten most abundant *de novo* repeat families, eight map to the Escribá insert across most of their lengths at sites that are consistently over-represented in DNA sequencing coverage and BLAST hits from other regions of the genome, and correspond to direct repeats of the ScRTE element, unclassified inverted and direct repeats, as well as hAT and Helitron elements (Figure 5E).

Transcriptome assembly and gene annotation

We annotated protein-coding genes in the Canu and Falcon genome assemblies with Maker2 (Holt and Yandell 2011) guided by transcriptome assemblies from poly-A enriched RNA-seq datasets from *Sciara* male and female embryos, larvae, pupae, and adults (Figure 3). With the gene sets available from each assembly, we performed a final set of reference-free evaluations to choose a final assembly: Canu or Falcon (Figure 3). The Falcon assembly had slightly longer contig size statistics and a corresponding lead in metrics from optical map alignments (Figure 5F, Supplemental Figure S13). However, the Canu assembly outperformed Falcon in completeness metrics, RNA-seq and *de novo* transcriptome alignments, as well as metrics from Illumina, PacBio, and MinION datasets (Figure 5F, Supplemental Figure S13). Moreover, both the Canu-guided transcriptome assembly and the transcripts in the final Canu annotation received higher evaluation scores than their Falcon counterparts (Figure 5F, Supplemental Tables S14, S15). Finally, the Canu annotation had lower annotation edit distances, more genes with GO terms, Pfam domains, and/or BLAST hits in the UniProt-SwissProt database, more BUSCOs, as well as more hits with proteomes from *Drosophila melanogaster* and

577 *Anopheles gambiae* (Figure 5F, Supplemental Figure S14, Supplemental Table S16). We
578 conclude that the Canu assembly had higher consistency with the genome sequencing datasets
579 and yielded the superior gene set. We therefore chose the Canu assembly as the first draft
580 genome for *Sciara coprophila.*
581
582 The final annotation of the Canu assembly had 23,117 protein-coding gene models with
583 28,870 associated transcripts (Supplemental Table S15A). There are more genes than expected
584 from other fly genomes, which may be a result of gene splitting in the annotation. To increase the
585 quality of the *Sciara* gene set, the annotation was deposited at the i5k-workspace for community-
586 enabled manual curation (https://i5k.nal.usda.gov/). Nevertheless, in its current form, the
587 annotation contains nearly all expected Dipteran genes: 94.2% complete Dipteran BUSCOs were
588 found in the final gene set, 97% when including fragmented BUSCOs (Supplemental Figure S14E,
589 Supplemental Table S15A). The majority of genes in the annotation (87.5%) had only a single
590 associated transcript isoform (Supplemental Figure S14B). The median gene and transcript
591 lengths are ~2.6 kb and ~1.3 kb, respectively (Supplemental Table S15A). Genes had a median
592 of 4 exons, ranging from just one (10.8% of genes) to over 100 exons. There are 10,801 genes
593 with both 5' and 3' UTRs annotated and 13,335 with one or the other. Exons, introns, 5' and 3'
594 UTRs had median lengths of 182 bp, 80 bp, 165 bp and 184 bp, respectively. Of all genes, we
595 were able to attach functional information to ~65%. Specifically, 8671 (37.5%) have Ontology
596 Terms, 13745 (59.5%) have UniProt/SwissProt hits, 13789 (59.6%) have Pfam descriptions (El-
597 Gebali et al. 2019), 8252 (35.7%) have all three, and 14961 (64.7%) have one or more
598 (Supplemental Figure S14F, Supplemental Table S16). Genes spanned over 54% of the Canu
599 assembly, mostly attributable to introns, and ~20% of the assembly was both unique (not
600 repetitive) and intergenic (Supplemental Figure S14H).
601

In the standard Dipteran model, *Drosophila melanogaster*, where males are XY and females are XX, male flies exhibit dosage compensation of X-linked genes. We used the *Sciara* gene annotation and anchoring information to explore dosage compensation in *Sciara.* The majority of cells in *Sciara* embryos, larvae, pupae, and adults are somatic where X ploidy differs between males and females. Males are haploid and females are diploid for the X, respectively. Both sexes are diploid for autosomes. We defined genes as X-linked if they were on contigs anchored into the X chromosome by the coverage analysis described above. We then determined if there was dosage compensation for X-linked genes, or if they consistently had 2-fold lower transcript abundances in male samples. Across each stage of development sequenced, the distributions of log2 fold changes between male and female transcript abundance were the same for autosomal and X-linked genes (Figure 5G, Supplemental Figure S15). There were many examples of both autosomal and X-linked genes that were differentially expressed between males and females, but there was no difference between males and females for the majority of genes in both classes. Therefore, the evidence strongly supports the existence of dosage compensation of most X-linked genes in *S. coprophila*.

DNA modification signatures in single-molecule data

The mechanism for imprinting in *Sciara* remains unknown. Since imprinting in mammals utilizes DNA methylation (Li et al. 1993), it was if interest to determine whether DNA modifications are present in *Sciara*. The gene annotation contains the proteins involved in cytosine and adenine methylation pathways (reviewed in Armstrong et al 2019; Rausch et al 2020) that are expected to be found in Dipterans, including putative homologs for DNMT2, TET-family proteins, DAMT-1/METTL4, N6AMT1, ALKBH1, jumu, and several proteins with methyl-CpG binding domains (Supplemental Table S17A-C). There was also evidence of DNA modifications in the *Sciara* genome found using anomalies in the raw signal of both single-molecule, long-read sequencing datasets (Flusberg et al. 2010; Clark et al. 2012; Simpson et al. 2017). The high-coverage PacBio

628 dataset was used to call site-specific modifications in the assembly for 5mC, 4mC, and 6mA. The
629 low-coverage MinION dataset was used to find kmers with signal distributions that were shifted
630 compared to expected models, which could result from DNA modifications. These kmers were
631 used to find sub-motifs for comparison to motifs obtained in the PacBio analysis.
632
633 Using the PacBio SMRT kinetics data, we estimated that ~0.13-0.24% of adenine sites in
634 the *Sciara* male embryo genome were potentially modified with up to ~0.04-0.06% of adenine
635 sites exhibiting the 6-methyl-Adenine (6mA) signature (Figure 6A**,** Supplemental Table S18A),
636 which is similar to 6mA densities seen for humans (~0.05%; Xiao et al. 2018), some fungi
637 (~0.05%; Mondo et al. 2017), *Drosophila embryos* (0.07%; Zhang et al. 2015), and pig (0.05%;
638 Liu et al. 2016). The tens of thousands of modified adenines were distributed ubiquitously
639 throughout the assembly, including in genes and repeats as well as on both autosomal and X-
640 linked sequences (Supplemental Figure S16A-C). Over 50% of the reads aligning to the majority
641 of 6mA sites were estimated to contain 6mA (Figure 6B), suggesting that while the mark may be
642 rare in the genome it is common at those sites. Although adenine modifications were found in
643 many dimer and trimer contexts, AG and GAG were most enriched (Figure 6C**,** Supplemental
644 Figure S16D, Supplemental Tables S19, S20**)**. GAG sites were modified up to 7-8 times more
645 frequently than the rate for A alone, with 0.9-1.7% GAG sites flagged as modified and 0.3-0.5%
646 flagged as 6mA specifically (Supplemental Table S18B). The frequencies of bases surrounding
647 the 6mA position in enriched 7mers showed a prominent 4 bp GAGG motif (Figure 6D), which did
648 not differ between X and autosomal sequences (Supplemental Figure S17). Other motifs
649 associated with 6mA in the *Sciara* genome included CAG within them (Supplemental Figure S18).
650 AG, GAG, GAGG, and CAG motifs were also previously found associated with 6mA sites in
651 human, rice, and *C. elegans* genomes (Greer et al. 2015; Xiao et al. 2018; Zhou et al. 2018). We
652 found that 6mers defined by the sequence logo from enriched 7mers showed shifted MinION
653 signal distributions whereas other control kmers fully agreed with the expected model (e.g.

654 CGAGGT; Figure 6E-F, Supplemental Figure S19). From the set of all kmers with shifted MinION
655 signals, we found similar motifs to those found in the analysis of 6mA sites identified in the PacBio
656 analysis (Figure 6G, Supplemental Figure S18).
657
658 We also used the PacBio SMRT kinetics data to look at cytosine methylation, which has
659 been previously shown to mark heterochromatic regions in *Sciara* chromosomes by
660 immunofluorescence (Eastman et al. 1980; Wei et al. 1981; Greciano et al. 2009). Up to 0.6-1.1%
661 of cytosines were modified with up to 0.11-0.24% and 0.26-0.43% showing 4-methylcytosine
662 (4mC) and 5-methylcytosine (5mC) signatures, respectively (Figure 6A, Supplemental Table
663 S17C). Modified cytosines were present throughout autosomal and X-linked sequences
664 (Supplemental Figure S16A-C). The frequency of methylation at the majority of 4mC and 5mC
665 sites was estimated to be over 80% (Figure 6B), despite being rare in the genome overall.
666 Modified cytosines were found in all dimer and trimers, but the most enriched were CG and GCG
667 (Figure 6C, Supplemental Figure S16D). This is reflected in the sequence logos constructed from
668 enriched 7mers centered on the modified C position (Figure 6D, Supplemental Tables S19, S20),
669 and was the same for autosomes and the X (Supplemental Figure S17). Up to ~1.3-2.5% of CpG
670 dinucleotides were estimated to be modified with 0.26-0.57% and 0.55-0.96% specifically
671 classified as 4mCpG and 5mCpG, respectively (Supplemental Table S18D). A more sensitive
672 algorithm (Suzuki et al. 2016) estimated as high as 6.4% of CpG dinucleotide sites in the genome
673 as targets for methylation in male *Sciara* embryos (Supplemental Table S18E). GCG sites were
674 modified up to ~4-5 times more frequently than the rate for C alone and 2 times more than CG,
675 with 2.5-4.9% of GCG sites flagged as modified and 0.5-1.2% and 0.9-1.5% of GCG sites flagged
676 as 4mC and 5mC, respectively (Supplemental Table S18F). Interestingly, GCG trimers are
677 depleted in the genome sequence whereas GTG trimers are enriched (Supplemental Figure S20).
678 This suggests that GCG may be a methylation target in the germline where 5mC deamination and
679 conversion to thymine can deplete GCG trimers over evolutionary time. We found that 6mers

680 defined by the sequence logos from enriched 7mers displayed shifted MinION signal distributions
681 (e.g. for TTCGGT and GGCGGA) whereas control kmers did not (Figure 6E-F, Supplemental
682 Figure S19), and that many motifs similar to those in the PacBio analysis specific to 4mC and
683 5mC were found when looking for motifs in kmers with shifted MinION signal distributions (e.g.
684 GCG; Figure 6G, Supplemental Figure S18).
685
686 The distribution of distances between adjacent DNA modifications, for both methylated C
687 and A, showed an enrichment of shorter distances than expected by chance (Figure 6H). There
688 were spikes of enrichment with a periodicity of 10 bp out to distances of at least 200 bp when
689 looking at both strand-agnostic and strand-specific spacings (Figure 6H, Supplemental Figures
690 S21-22). This periodicity is highly suggestive of turns of the DNA helix. Periodic spacing of 10 bp
691 between methylation sites and target motifs has been observed enriched over nucleosome
692 positions in *Arabidopsis* and mammals (Jia et al. 2007; Chodavarapu et al. 2010; Collings and
693 Anderson 2017). Moreover, 6mA was shown to be phased between nucleosomes in
694 *Chlamydomonas* and *Tetrahymena* (Fu et al. 2015; Wang et al. 2017; Luo et al. 2018). Indeed,
695 ~175 bp is one of the most enriched distances separating two modifications in our *Sciara* male
696 embryo data (Figure 6H, Supplemental Figures S21-22), a length reminiscent of nucleosomal
697 spacing in general and the exact length found for nucleosome intervals in *Drosophila* (Mavrich et
698 al. 2008).
699
700 We searched for relationships between DNA modifications and genomic features. The
701 trends were the same for all modification types (6mA, 4mC, 5mC). With respect to annotated
702 protein-coding genes, DNA modifications were random or slightly depleted, though there were
703 slight depletions in exons and promoters and slight enrichments in introns (Supplemental Figure
704 S16B, Supplemental Table S21A-B). These trends were the same when using gene locations
705 defined by the StringTie transcriptome assembly (Supplemental Table S21C) and were generally

706 true even when splitting the genes into categories of not expressed, lowly expressed, and highly
707 expressed using male embryo RNA-seq data (Supplemental Table S21D). Repeat regions in the
708 genome had more modifications than expected, and conversely the non-repeat regions had fewer
709 than expected (Supplemental Figure S16B, Supplemental Table S21E-F). In the *de novo* repeat
710 library, there were repeat families, including simple repeats, with 2-100 fold more modifications
711 than expected and many families with no modifications indicating that specific classes of repeats
712 are targeted for DNA methylation.
713
714 **Candidate germline-limited L sequences:**
715 L chromosome sequences are likely to be absent or of very low abundance in our datasets
716 from late male embryos. Nevertheless, an effort was made to identify candidate L-sequences.
717 Similar to identifying X-linked contigs in the assembly based on haploid-level coverage, L
718 candidates were gathered based on very low coverage, which may include junk or redundant
719 contigs. There were 25 contigs summing to ~230 kb that had at most 3X PacBio coverage across
720 their lengths in contrast to the genomic average of ~34X. These sequences were comprised of
721 ~60% repeats compared with ~40% genome-wide. The most abundant repeats were unclassified,
722 but Gypsy, Pao, and Zator transposons were highly represented. There were 15 mRNA isoforms
723 annotated in these low-coverage contigs corresponding to 13 genes (Supplemental Table S22).
724 Seven genes had putative functional information. Six had best hits to UniProt-SwissProt proteins
725 corresponding mostly Drosophila proteins, including Facilitated trehalose transporter Tret1, Ras-
726 related protein Rab-3, Ubiquitin carboxyl-terminal hydrolase 36, RNA-directed DNA polymerase
727 (jockey reverse transcriptase), Vitellogenin-2, Rho GTPase-activating protein. One was a protein
728 of unknown function, but was classified in the ribosomal L22e protein family from the Pfam domain
729 analysis.
730

An additional attempt to identify L candidate sequences was made by rescuing unassembled reads. Since sequences of relatively low abundance may not have been assembled, short and long reads that do not map to the Canu *Sciara* genome assembly were used to generate new assemblies using Platanus and Canu, respectively. Using the unmapped long reads, Canu returned 250 contigs summing to 2.55 Mb in length and 2247 unassembled reads summing to 7.45 Mb for a total of 10 Mb. The majority of the sequences were identified as bacterial: 89% of the total contig length and 69% of the total unassembled length for a total of 7.4 Mb of bacterial sequence (Supplemental Figure S23). Similarly, when assembling the unmapped short read pairs, Platanus returned 330 scaffolds summing to 6.8 Mb, and ~96% was identified as bacterial (Supplemental Figure S23).

We focused on the 698 long-read sequences (1.7 Mb) and the 159 short-read scaffolds (141.5 kb) that were either identified as Arthropod or had no hits and 20-45% GC content (Supplemental Figure S23). Only 12% of the total length of these sequences aligned to the assembly, and just 14.5% and 28.3% of the targeted long-read and short-read sequences were identified as repeats. The most abundant repeats present were unclassified. The repeats were also enriched for simple repeats as well as transposons, such as Helitron (RC), Pao (LTR), RTE (LINE), Jockey (LINE), and Mariner (DNA). The centromere-associated Sccr repeat (Escribá et al 2011) was on 14 contigs. There were also contigs with rDNA and rDNA transposons R1 or R2. A small fraction of short reads contained the peri-centromeric tandem repeat B4 (Escribá et al 2011). Neither B4 nor rDNA has been observed on L chromosomes by in situ hybridization (Escribá et al 2011), suggesting that at least some of these sequences are not from L chromosomes. About 8% of the combined long- and short-read sequence length was covered by hits from 116 proteins, 16% of which were transposon-related and another 65% of which had other functional information. The most convincing alignments matched proteins (Supplemental Figure S23), such as (i) an Integrator complex subunit that is involved in snRNA transcription and

757 processing, (ii) two zinc-finger transcription factors, (iii) a TATA-box binding protein, (iv) proteins
758 involved with chromosome cohesion, recombination, and segregation like Wings apart-like protein
759 (WAPL), Structural maintenance of chromosomes protein 6 (SMC6), and MOB kinase activator-
760 like 1 (mats), and (v) proteins involved in the nervous system. The majority of these were on
761 contigs with no matches to the genome assembly.

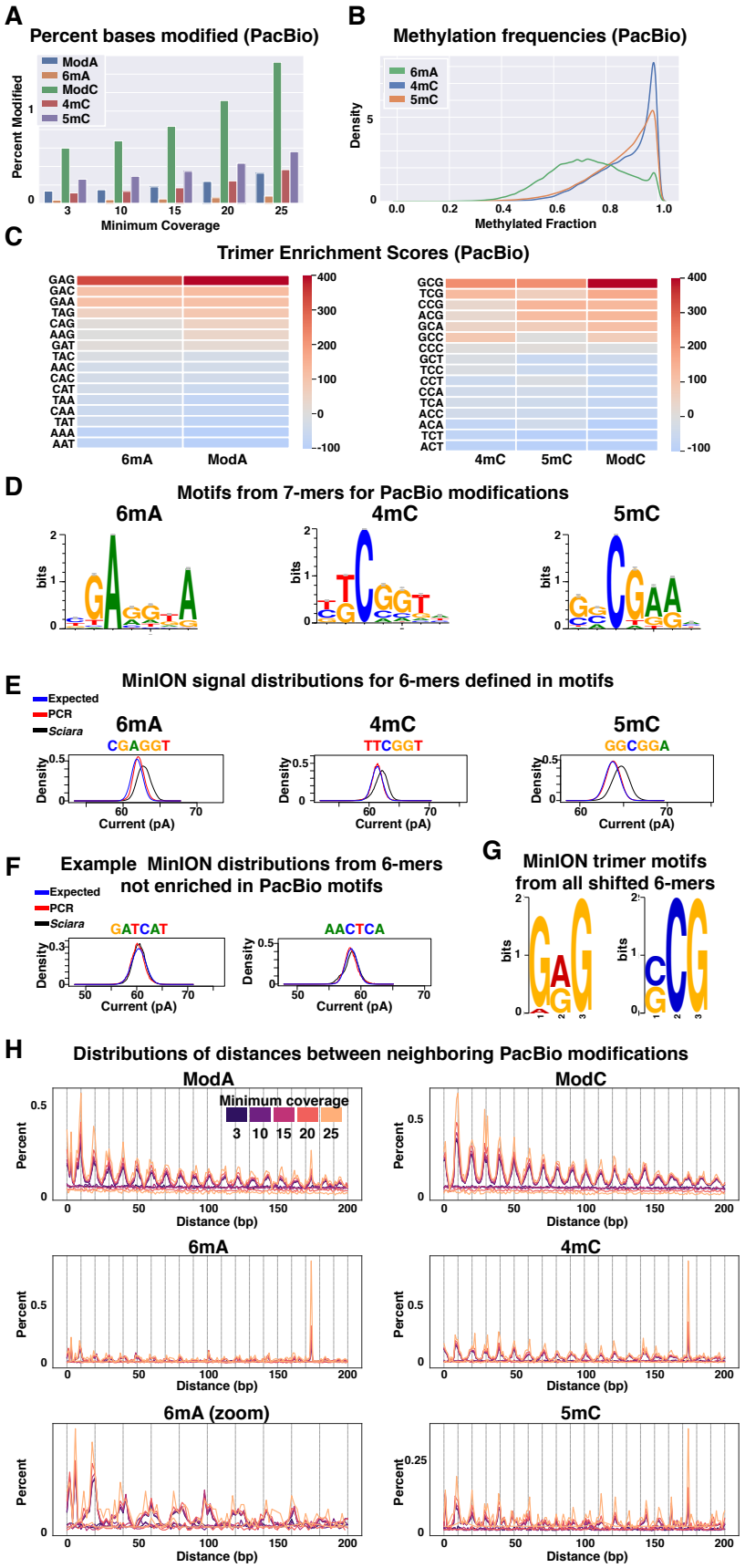

Figure 6: DNA modifications in male embryo genomic DNA of *Sciara coprophila*

(A) Percent of adenines or cytosines assigned to a modification class given a minimum coverage level in the PacBio analysis. ModA and ModC are the sets of all adenines or cytosines, respectively, flagged as modified whereas 6mA, 4mC, and 5mC are the subsets of adenines or cytosines therein with those specific classifications.

(B) Methylation frequencies from the PacBio analysis at sites classified as having the given methylation type.

(C) Chi-square standardized residuals (enrichment scores) indicating how many standard deviations away each observation is from expectation for trimers with middle adenines or middle cytosines from the PacBio analysis.

(D) Position weighted motifs from the sets of 7-mers (where the modified base occurs at position 3) enriched for 6mA, 4mC, or 5mC.

(E) The distribution of ionic current means from the MinION data for 6-mers defined by the PacBio motifs in (D). The blue line shows the expected distribution given the MinION model for each kmer. The red line shows the distribution learned from whole *E. coli* genome PCR data (Simpson et al. 2017) using only canonical nucleotides. The black line shows the distribution learned from native genomic DNA from *Sciara*. Distributions are from template reads.

(F) As in (E), but showing examples of 6-mers not defined by motifs learned in the PacBio analysis.

(G) Two of the top three trimer motifs learned from the set of all 6-mers that had shifted MinION signal distributions with respect to the expected models.

(H) Distributions of distances between

762

DISCUSSION

Derivation of the *Sciara* genome and anchoring

We report here the assembled sequence of the male somatic genome of the lower Dipteran fly, *Sciara coprophila*, as well as its gene annotation from transcriptomes covering both sexes and all life stages. To find the assembly approach that worked best for the *Sciara* genome, we used a battery of reference-free metrics to evaluate assemblies generated from different technologies, algorithms, inputs, and parameters. *Sciara* genome sequences assembled with Canu and Falcon from a blend of PacBio and MinION data, and polished with PacBio and Illumina data, performed best and were selected for scaffolding using optical maps from the BioNano Genomics Irys platform. Ultimately, the Canu scaffolds were the final selection for the first draft sequence owing to their higher quality gene annotation. This release of the *Sciara* male somatic genome assembly contains 299 Mb of sequence on 205 primary contigs with 50% of the expected genome size on only 12 scaffolds that range from 8.2-23 Mb long. Annotating the *Sciara* protein-coding genes with guidance from RNA-seq data gave a gene set that contained 97% of Dipteran BUSCOs, suggesting it is essentially complete. We have anchored a significant amount of the *Sciara* genome sequence on the three autosomes using previous *in situ* hybridization data, accounting for 20-46% of chromosome II, 8-19% of chromosome III and 37-52% of chromosome IV. As *Sciara* male somatic cells have only one X chromosome in contrast to two of each autosome, we were able to use coverage levels in addition to *in situ* hybridization to anchor most or all of the X chromosome sequences. In total, ~137-138 Mb of sequence, or ~49% of the expected genome size, was anchored into chromosomes. Future research with targeted approaches to study the L chromosome and variations associated with the X' chromosome will be of interest beyond the current male somatic genome assembly presented here.

In its current state, the *Sciara* genome assembly is already more contiguous than up to 95% of all Arthropod genomes described (http://i5k.github.io/arthropod_genomes_at_ncbi). Its contiguity statistics exceed 42 of the 43 currently available lower Dipteran genome assemblies, over 75% of which have sub-100 kb N50s. The low contiguity of most available Dipteran genome sequences and the lack of anchoring to chromosomes limits their utility. However, the *Sciara* genome assembly presented here may be useful for scaffolding currently available and future *Nematoceran* genomes by synteny. The long contigs in the *Sciara* genome assembly reflect the success of using long read technologies and optical maps, both of which span repeats. The long-read datasets and the resulting assembly will be important and extremely useful for analyzing regions of repetitive DNA, like rDNA, centromeres, telomeres, and transposable elements.

Comparative phylogenomics

Comparative genomics provides an understanding into the rates and patterns of evolution of genes as well as populations and species (Wiegmann and Richards 2018). The phylogenetic position of *Sciara (Bradysia) coprophila* makes its genome and transcriptome sequences valuable for future comparative genomics studies. *Sciara* is a lower Dipteran fly (Nematocera) whereas *Drosophila* is a higher Dipteran fly (Brachycera) and they diverged from one another ~200 MYA (Wiegmann et al 2011). The *Sciara* genome size of 280 Mb (362 Mb with the L chromosomes) is larger than the 175 Mb size of the *Drosophila melanogaster* genome (Elllis et al 2014), but similar to the 264 Mb genome of the Nematoceran *Anopholes gambia* (Sharakhova et al 2007). Dipteran phylogenetics has been much studied (Hennig 1973; McAlpine and Wood 1989) but some unresolved questions remain. Previously, morphological criteria suggested that the Brachycera (containing *Drosophila*) and the Nematocera (containing *Sciara*) diverged from a common ancestor. However, more recent molecular data supports a model where the Nematoceran infraorder Bibionomorpha ultimately gave rise to the Brachycera (Wiegmann et al 2011). The *Sciara* genome and transcriptome sequences reported here will be valuable resources to further

814 describe Dipteran phylogenetic relationships, and will further our understanding of the evolution
815 and molecular structure of genes and pathways in Dipterans including Drosophila.
816
817 **Evolution of sex determination**
818 The evolution of sex determination is a topic of much current interest. The most common
819 occurrence is male heterogamety where males are XY and females are XX. In contrast, in female
820 heterogamety, females have heteromorphic sex chromosomes (e.g., ZW), and males are
821 homomorphic (e.g., ZZ). Female heterogamety is rare in insects (Blackmon et al 2017), but is
822 exhibited by *Sciara* where males have a single X in their soma and females have two (Gerbi
823 1986). Female *Sciara* can be either XX or X'X where the X' chromosome carries a long paracentric
824 inversion that inhibits crossing over with the X. Thus, the heterogametic *Sciara* female determines
825 the sex of her offspring. In *Sciara coprophila*, XX mothers have only sons and X'X mothers have
826 only daughters. Presumably, the ooplasm is conditioned by the *Sciara* mother to determine the
827 sex of the offspring via X chromosome elimination. In agreement with this hypothesis, sex is
828 determined by a temperature-sensitive maternal effect that controls X-chromosome elimination in
829 *Sciara ocellaris* (Nigro et al. 2007). As for the single X in male soma, *Sciara* males are haploid
830 only for the X but diploid for the autosomes, unlike haplodiploid males that are haploid for their
831 entire genome. This is accomplished by X chromosome elimination in the early *Sciara* embryo
832 and was noted by White (1949) to occur in the Nematoceran families of Sciaridae and
833 Cecidomyidae (including the Hessian fly *Mayetiola destructor*). Comparisons of the
834 genomes/transcriptomes of *Sciara* and *M. destructor* might help to elucidate the molecular
835 regulation of X chromosome elimination.
836
837 Cytoplasmic sex determination, as suggested above for *Sciara*, occurs if sex is under the
838 control of cytoplasmic elements, such as endosymbionts. *Wolbachia* and *Rickettsia* are related
839 groups of intracellular alpha proteobacteria that can distort the sex ratio of their arthropod hosts

(Lawson et al, 2001, Serbus et al 2008). They are transmitted through the egg cytoplasm and alter reproduction in their arthropod hosts in various ways, including cytoplasmic incompatibility, feminization of genetic males, and male killing (Werren and Windsor 2000; Serbus et al 2008). Both can induce parthogenesis (Blackmon et al 2017). The latter is of interest since (i) parthenogenetic *Sciara* embryos have been observed, but their development arrests in embryogenesis (de Saint Phalle and Sullivan 1998), and (ii) although we did not find *Wolbachia* sequences in *Sciara* genomic DNA, we essentially co-assembled an entire *Rickettsia* genome. Moreover, our genomic copy number analyses suggest there are two *Rickettsia* cells per *Sciara* cell on average in 1-2 day old male embryos. Further evidence is needed to ascertain if *Rickettsia* plays a role in *Sciara* sex determination.

Paternal chromosome imprinting

The first example of a chromosome or a chromosomal locus "remembering" its maternal or paternal origin was noted in *Sciara* and the term "imprinting" was coined (Crouse 1960). Specifically, in *Sciara* male meiosis I, the paternally derived chromosomes move away from the single pole of the naturally occurring monopolar spindle and are discarded in a bud of cytoplasm. This is an example of paternal genome elimination (PGE) that can give rise to haplodiploidy in other systems (Blackmon et al 2017). Thus, only the maternal genome is passed down through sperm in *Sciara*. Although sperm in *Sciara* is haploid for autosomes, it is diploid for the X chromosomes due to non-disjunction of the X in *Sciara* male meiosis II (Gerbi 1986). After fertilization of the haploid egg, diploidy is re-established for the autosomes, but the X chromosome is temporarily triploid. Either one or both copies of the paternally-derived X are eliminated from female or male embryos, respectively, during the 7^{th}-9^{th} embryonic cleavage division, representing another example of imprinting in *Sciara* (de Saint Phalle and Sullivan 1996). Nevertheless, the mechanism for imprinting in *Sciara* remains elusive. It is of interest to learn if DNA modifications occur in *Sciara* since different imprints in mammalian genomes are laid down in eggs and sperm

866 through a DNA methylation mechanism, leading to differential gene expression at imprinted loci
867 in the offspring (Li et al 1993).
868
869 DNA methylation typically occurs at CpG sites where it is established *de novo* by DNA
870 methyltransferase 3 (DNMT3) and is maintained by DNMT1 (Goll and Bestor 2005, Kato et al
871 2007). In contrast to vertebrates, DNA methylation in invertebrates is relatively sparse (Bird 1980).
872 DNMT1 is found in all orders of insects except Diptera, which also lack DNMT3 (Bewick et al
873 2017). In agreement, our gene annotations suggest that *Sciara* also lacks DNMT1 and DNMT3.
874 Some bisulfite sequencing studies revealed that CpG DNA methylation is found in all insect
875 Orders except Dipteran flies (Bewick et al 2017) and failed to find specific patterns for methylated
876 C in *Drosophila* embryos (Zemach et al 2010; Raddatz et al 2013). Other studies have asserted
877 that *Drosophila melanogaster* has DNA methyltransferase activity and CpC methylation (Panikar
878 et al 2015), has low levels of 5-methylcytosine (5mC) (Capuano et al 2014, Takayama et al 2014,
879 Deshmukh et al. 2018), and has more cytosine methylation in stage 5 *Drosophila* embryos than
880 oocytes (Takayama et al 2014). Moreover, 6-methyladenine (6mA) has been recently reported to
881 be in the genomic DNA of *Drosophila* and other eukaryotes (Fu et al. 2015; Greer et al. 2015;
882 Zhang et al. 2015; Liu et al. 2016; Mondo et al. 2017; Wang et al. 2018; Xiao et al. 2018). Typically,
883 the level of 6mA is quite low, such as 0.001% in *Drosophila* but rises to 0.07% in early embryos
884 (Zhang et al 2015). DAMT-1 appears to be the methyltransferase for 6mA in insect cells and
885 DMAD has 6mA demethylating activity in *Drosophila* (Luo et al 2015, Zhang et al 2015). Our gene
886 annotations suggest that *Sciara* has both DAMT-1 and DMAD.
887
888 Before it can determined whether or not imprinting in *Sciara* involves DNA modifications,
889 it needs to be determined if the *Sciara* genome harbors DNA modifications at all. Previous
890 immunofluorescence studies have suggested the presence of 5-methylcytosine in *Sciara*
891 chromosomes (Eastman 1980, Greciano 2009). Similarly, our sequencing data support the

892 presence of base modifications in the *Sciara* genome. Overall, up to 0.6-1.1% of cytosines may
893 be modified in the *Sciara* genome, especially at GCG sites, with specifically 0.1-0.2% and 0.3-
894 0.4% identified as 4mC and 5mC, respectively. In addition, 0.13-0.24% of adenine sites in the
895 *Sciara* male embryo genome were potentially modified with up to ~0.04-0.06% of adenine sites
896 containing 6mA, especially GAG sites. Moreover, the PacBio analysis suggests that these DNA
897 modifications are phased with 10 bp and 175 bp periodicities, suggesting physical interactions
898 between the 10 bp turns of the DNA helix and methylation machinery as well as relationships with
899 nucleosome spacing, both of which have been seen previously using orthogonal methods (Jia et
900 al. 2007; Chodavarapu et al. 2011; Fu et al. 2015; Collings and Anderson 2017; Wang et al. 2017;
901 Luo et al. 2018). Lastly, the distribution of modifications we observed with respect to genes and
902 repeats are concordant with previous observations (i) of methyl-C in *Drosophila* (Takayama et al.
903 2014) and (ii) that heterochromatic regions of the *Sciara* genome, where most repeats reside, are
904 enriched for 5mC (Eastman et al. 1980; Greciano et al. 2009). Overall, the evidence from single-
905 molecule sequencing lends support to the presence of methylated cytosines and adenines in the
906 autosomes and X chromosome in the male embryo genome of *Sciara*. However, the analyses
907 suggest that the levels of DNA modifications are low. Their abundance in females and other
908 developmental stages and tissues as well as their biological significance remains to be
909 determined in future investigations. Nevertheless, given the evidence from the current study and
910 previous work, base modifications may be a promising avenue for the study of imprinting in *Sciara*.
911
912 **Summary**
913 The *Sciara* genome sequence provides a foundation for future studies to delve into the
914 many unique biological properties of *Sciara* (reviewed by Gerbi 1986) that include **(i)** chromosome
915 imprinting; **(ii)** sex determination by the mother; **(iii)** a monopolar spindle in male meiosis I; **(iv)**
916 non-disjunction of the X chromosome in male meiosis II; **(v)** chromosome elimination in early

917 embryogenesis; **(vi)** germ line limited L chromosomes; **(vii)** DNA amplification in late larval
918 salivary gland polytene chromosomes; **(viii)** high resistance to radiation.

METHODS

Tissue collection, DNA extraction, and DNA sequencing:

Sciara coprophila (renamed *Bradysia coprophila)* was used for these studies. *Sciara* (stock: Holo2) matings were performed to produce only male offspring from which embryos aged 2 hours – 2 days (genome sequencing datasets) or pupae (BioNano Irys genome mapping datasets) were collected. For a minority of MinION sequencing data, adult males were used. Genomic DNA (gDNA) was isolated using DNAzol (ThermoFisher) as per the manufacturer's instructions with some modifications. gDNA was cleaned with AMPure beads (Beckman Coulter). Purity was checked with NanoDrop (ThermoFisher) and concentration was checked with Qubit (ThermoFisher).

For Illumina HiSeq 2000 sequencing, male embryo gDNA was sonicated to a size range of 100-600 bp, prepared using the NEBNext kit (New England Biolabs) following the manufacturer's directions, run on a 2% NuSieve agarose (Lonza) gel, size-selected near the 500 bp marker, gel purified (Qiagen), and sequenced to obtain 100 bp paired-end reads.

For Pacific Biosciences RSII Single Molecule Real Time sequencing datasets (P5-C3 chemistry), male embryo gDNA was given to the Technology Development Group at the Institute of Genomics and Multiscale Biology at the Icahn School of Medicine at Mount Sinai for library construction and sequencing. Two DNA libraries were prepared and sequenced across 24 SMRTcells as described further in the Supplemental Methods.

MinION data was collected using multiple early iterations of the technology (original MinION and MkI), kits (SQK-MAP002, MAP004, MAP005, MAP006), and pores (R7.3 and R7.3 70 bps 6mer). We prepared 15 libraries from male *Sciara* embryo gDNA (making up >97% of the

945 data) and 2 from male adult gDNA. The manufacturer's instructions were followed with
946 modifications to increase read lengths (Urban et al. 2015 and Suppl. Methods). Libraries were
947 loaded onto the MinION, sequenced, and basecalled with Metrichor. Reads were extracted from
948 Fast5 files and analyzed using our own custom set of tools (Fast5Tools:
949 github.com/JohnUrban/fast5tools).
950
951 For BioNano Genomics (BNG) Irys optical maps, male pupae were flash frozen ground in
952 liquid nitrogen and high molecular weight gDNA was isolated (Suppl. Methods), nicked with BssSI
953 (CACGAG, New England BioLabs), labeled, and repaired according to the IrysPrep protocol
954 (BioNano Genomics).
955
956 **Genome assemblies**
957 After optional trimming/filtering with Trimmomatic (Bolger et al 2014) and/or error-
958 correction with BayesHammer (Nikolenko et al 2013), short-read assemblies were generated
959 using ABySS (Simpson et al. 2009), Megahit (Li et al. 2015), Platanus (Kajitani et al. 2014), SGA
960 (Simpson and Durbin 2010), SOAP (Luo et al. 2012), SPAdes (Bankevich et al. 2012), Velvet
961 (Zerbino and Birney 2008). Hybrid assemblies were generated using DBG2OLC (Ye et al. 2016)
962 and PBDagCon (http://bit.ly/pbdagcon) starting with Platanus contigs and long reads. Non-hybrid
963 long-read assemblies were generated with Canu (Koren et al. 2017), Falcon (Chin et al. 2016),
964 Miniasm (Li 2016) with RaCon (Vaser et al. 2017), ABruijn (Lin et al. 2016), and SMARTdenovo
965 (https://github.com/ruanjue/smartdenovo). For all assemblers, we varied filtering, error correction,
966 inputs, and parameters as detailed further in the Suppl. Methods. Long-read assemblies were
967 polished with Quiver (Chin et al. 2013) and Pilon (Walker et al. 2014). BlobTools (Laetsch and
968 Blaxter 2017) was used to identify contaminating contigs.
969
970 **Assembly evaluations**

Assembly evaluations included subsets of the following: contig size statistics, percent of Illumina reads that mapped using Bowtie2 (Langmead and Salzberg 2012), probabilistic scores from LAP (Ghodsi et al. 2013) and ALE (Clark et al. 2013), number of features from FRC^{bam} (Vezzi et al. 2012), percent error-free bases and/or the mean base score from REAPR (Hunt et al. 2013), completeness of gene content with BUSCO (Simão et al. 2015), the percent of long reads that aligned with BWA (Li and Durbin 2009), the average number of split alignments per long read, structural variations using Sniffles (Sedlazeck et al. 2018), the percent of raw BioNano map alignments using Maligner (Mendelowitz et al. 2015), the resulting optical map alignment M-scores, the number of bases covered by optical maps (span), and the total coverage from aligned optical maps. Evaluations were automated and parallelized on SLURM with a custom package (github.com/JohnUrban/battery).

Scaffolding

For hybrid scaffolding, optical maps >150 kb were assembled into consensus maps (CMAPs) using BioNano Pipeline Version 2884 and RefAligner Version 2816 (BioNano Genomics). Each selected assembly was used with the BNG CMAPs to create genome-wide hybrid scaffolds using hybridScaffold.pl version 4741 (BioNano Genomics). Quiver and PBJelly (English et al. 2012) were used to polish and gap-fill the scaffolds. PBJelly was used additionally to join more scaffolds with long-read evidence into “meta-scaffolds”, and Quiver and Pilon were used for final polishing.

Assembly anchoring

Haplotigs were identified using Minimap2 (Li 2018) and purge_haplotigs (Roach et al. 2018). To anchor contigs into chromosomes, sequences that were previously mapped to chromosomes experimentally were mapped to the assemblies using BLAST (Altschul et al. 1990). Differentiating between autosomal and X-linked contigs was performed by requiring haploid

997 coverage levels across at least 80% of a contig to be called as X-linked (else autosomal), using
998 Minimap2 and BEDTools (Quinlan and Hall 2010).
999
1000 **Transcriptome assemblies**
1001 For strand-specific RNA-sequencing libraries, poly-A RNA was prepared from a given sex
1002 and stage using TRIzol (Invitrogen/Thermofisher), DNase (Qiagen), RNeasy columns (Qiagen),
1003 and Oligo-dT DynaBeads (Life Technologies). RNA integrity was evaluated on 1.1%
1004 formaldehyde 1.2% agarose gels. RNA purity and quantity were measured with the NanoDrop
1005 (ThermoScientific) and Qubit (ThermoFisher) throughout. Libraries were prepared from poly-A
1006 RNA using NEB's Magnesium Fragmentation Module, SSIII (Invitrogen) first strand synthesis with
1007 random primers, NEBNext Second Strand Synthesis module with ACGU nucleotide mix (10 mM
1008 each of dATP, dCTP, dGTP, and 20 mM of dUTP), NEBNext End Repair and dA-Tailing (NEB),
1009 and ligation (NEB: NEBNext Quick Ligation Reaction Buffer, NEB Adaptor, Quick T4 Ligase). The
1010 libraries were size-selected with AMPure beads (Beckman Coulter). Uracil-cutting for strand-
1011 specificity (and hairpin adapter cutting) was performed with NEBNext USER enzyme, followed by
1012 PCR using NEBNext High-Fidelity 2X PCR Master Mix and NEBNext indexed and universal
1013 primers for 12 cycles. A final size-selection of PCR products was performed with AMPure beads.
1014 Purity, quantity, and size of the libraries were checked with NanoDrop, Qubit and Fragment
1015 Analyzer (Agilent). Traces suggested the mean estimated fragment sizes was around 420 bp,
1016 indicating mean insert sizes near 300 bp. Libraries were sequenced to yield 100 bp paired-end
1017 reads using the Illumina HiSeq 2000. The strand-specific RNA-seq datasets were combined and
1018 assembled with Trinity (Grabherr et al. 2011) or using HiSat2 (Kim et al. 2019) and StringTie
1019 (Pertea et al. 2015). Transcriptome assemblies were evaluated with BUSCO (Simão et al. 2015),
1020 RSEM-Eval (Li et al. 2014), and TransRate (Smith-Unna et al. 2016).
1021
1022 **Repeat and gene annotation**

Species-specific repeat libraries were built using RepeatModeler (Smit and Hubley 2008). These were combined with previously known repeat sequences from *Bradysia coprophila* as well as all Arthropod repeats in the RepeatMasker Combined Database: Dfam_Consensus-20181026 (Hubley et al. 2016), RepBase-20181026 (Bao et al. 2015). To predict protein-coding genes, Maker2 (Holt and Yandell 2011) was used with transcriptome evidence described above, transcript and protein sequences from related species for homology evidence, Augustus (Hoff and Stanke 2019), SNAP (Korf 2004), GeneMark-ES (Ter-Hovhannisyan et al. 2008), and RepeatMasker (Smit et al. 2013) with repeat libraries described above. InterProScan (Quevillon et al. 2005) was used to identify Pfam domains and GO terms from predicted protein sequences, and BLASTp was to find the best matches to curated proteins in the entire UniProtKB/Swiss-Prot database (The UniProt Consortium 2019). Maker2 transcriptomes were evaluated using annotation edit distances, BUSCO, RSEM-Eval, and TransRate.

DNA modification analyses

PBalign (github.com/PacificBiosciences/pbalign) with BLASR v2 (Chaisson and Tesler 2012) was used to align PacBio reads to the entire unfiltered assembly to avoid forcing incorrect mappings. Pbh5tools (github.com/PacificBiosciences/pbh5tools) was used to merge and sort the mapped reads. ipdSummary from kineticsTools v0.6.0 (github.com/PacificBiosciences/kineticsTools) was used to predict base modifications across the Canu genome assembly (--pvalue 0.01 --minCoverage 3 --methylMinCov 10 --identifyMinCov 5). AgIn (Suzuki et al. 2016) was also used to look at CpG methylation. For all analyses on predicted DNA modifications, we used only primary contigs labeled as Arthopoda. Kmer enrichment scores for dimers and trimers were obtained from the Chi-square standardized residuals found when comparing the distribution of kmers that had a specific modification at a fixed position with the genome-wide distribution of kmers with the target base at that position. We also used this approach to define enriched 7-mers for position weight matrix motifs using WebLogo (Crooks et

al. 2004). In addition, the 9 bp sequences centered on the top 500 or 5000 scoring specific modification calls were used with MEME (Bailey and Elkan 1994) to identify motifs using a second order Markov model background file trained on the *Sciara* genome assembly (fasta-get-markov -m 2 -dna). We determined if DNA modifications were enriched/depleted in various genomic regions using binomial models. When separating genes by expression level for this analysis, Salmon (Patro et al. 2017) was used to quantify expression over our Maker2 protein-coding gene annotation using male embryo RNA-seq. BEDtools was used to obtain spacing distances between modified bases as well as between random bases of the same type (e.g. m6A vs random A). Although 10 bp periodicities were obvious by visual examination, we formally determined the periodicities observed in counts of inter-modification distances between 0-200 bp by running a discrete Fourier transform (DFT) analysis using the Fast Fourier Transform (FFT) from Python's Numpy package.

For the MinION analysis, only datasets generated from the MkI, SQK-MAP006 kit, and R7.3 70 bps 6mer pore model were used, and only reads that aligned to primary contigs annotated as Arthropoda. We compared the signal distributions for each kmer in our *Sciara* dataset to the expected ONT kmer models, and to a MinION dataset generated from whole genome PCR on *E. coli* genomic DNA using the same kit and pore model (BioProject PRJEB13021; Run ERR1309547; www.ebi.ac.uk/ena; Simpson et al. 2017). MinION reads were aligned with BWA. Nanopolish (Simpson et al. 2017) was used to learn updated kmer models from the native *Sciara* and E. coli PCR MinION datasets. MEME was used to identify short motifs in all 6mers that differed from the expected ONT model.

Further bioinformatics

The Supplemental Methods contains software versions, as well as further details and exact commands for: read processing, genome assembling, polishing, evaluating, scaffolding,

gap filling, bacterial filtering, haplotig filtering, anchoring, transcriptome assemblies and evaluations, repeat library construction, repeat-masking, training gene predictors, alternative transcript and protein evidence, Maker2 iterations and evaluations, and the PacBio and MinION DNA modification analyses. Bioinformatics analyses were largely aided by custom scripts located at github.com/JohnUrban/sciara-project-tools, github.com/JohnUrban/fast5tools, github.com/JohnUrban/battery, github.com/JohnUrban/lave, and github.com/JohnUrban/fftDnaMods.

DATA ACCESS

Raw Illumina (DNA and RNA-seq), PacBio, MinION, and BioNano data generated in this study as well as BioNano CMAPs and PacBio kinetics and DNA modification results have been submitted to the NCBI BioProject database (http://www.ncbi.nlm.nih.gov/bioproject/) under accession number PRJNA123456. This Whole Genome Shotgun project has been deposited at DDBJ/ENA/GenBank under the accession VSDI00000000, and the Canu assembly version selected as the first draft genome release in this paper (Bcop v1.0) is version VSDI01000000. The automated Bcop_v1.0 annotation for the Canu assembly is available at the i5k Workspace (i5k.nal.usda.gov) where manual curation updates will be made.

DISCLOSURE DECLARATION

JMU and SAG were members of the MinION Access Program and received free reagents from ONT. JMU was also a member of the MinION Access and Reference Consortium (MARC) that conducts experiments partially funded by ONT.

ACKNOWLEDGMENTS

We thank Oxford Nanopore for early access to the MinION and for strong continual support, particularly from Michael Micorescu, Sissel Juul, Daniel Turner, Stuart Reid, David

Stoddart, Margherita Coccia, Richard Ronan, and Jackie Evans. We thank the members of the nanopore community, and particularly members of the MinION Access and Reference Consortium (MARC), for lively discussions. Thanks to Benjamin Raphael for helpful discussions on genome assembly and the Center for Computational Molecular Biology (CCMB) at Brown University for providing computing resources for our MinION. We thank the Technology Development Group at the Institute of Genomics & Multiscale Biology at the Icahn School of Medicine at Mount Sinai, particularly Gintaras Deikus for help in obtaining PacBio data, and Ali Bashir and Robert Sebra for discussions on PacBio chemistries, and genome assembly. Thanks to Adam Phillippy, Sergey Koren, and Brian Walenz for helpful correspondence and guidance about Canu and genome assembly in general. Thanks to Mark Howison, Stefano Lonardi and Stephen Richards for helpful correspondence and sharing experiences with various assemblers and tools. Thanks to Jared Simpson for providing guidance on Nanopolish. Thanks to Jennifer Urban for help drawing *Sciara* cartoons, to Yutaka Yamamoto for *Sciara* photographs, and to Miiko Sokka, Steven DeLuca, Ethan Greenblatt, and other members of the Spradling and Gerbi laboratories for useful discussions and comments. Thanks to Kevin Urban at Early Signal for valuable insights on FFT analysis. Thanks to the Center for Computation and Visualization (CCV) at Brown University, NSF EPSCoR, and Carnegie Science's Scientific Computing Committee for High-Performance Computing for computational resources and support. This work was supported by NSF/MCB-1607411 and NIH/GM121455 to SAG; predoctoral traineeships to JMU from NIH/T32-GM 007601, NSF/EPSCoR #1004057, and NSF predoctoral fellowship GRFP-DGE-1058262; NIH/P20 GM103418 to SJB; and funding through the Howard Hughes Medical Institute (ACS, JMU).

AUTHOR CONTRIBUTIONS

John Urban (JMU) collected all embryos, larvae, pupae, and adult Sciara needed for all experiments. JMU prepared all MinION libraries and performed all MinION sequencing and

analyses. JMU wrote the suites of tools for working with MinION data (https://github.com/JohnUrban/fast5tools), automating the battery of assembly evaluations (https://github.com/JohnUrban/battery), genome alignment visualizations (https://github.com/JohnUrban/lave), and all general bioinformatics over the course of this project (https://github.com/JohnUrban/sciara-project-tools). JMU obtained high molecular weight genomic DNA and delivered it to the Technology Development Group at the Institute of Genomics & Multiscale Biology at the Icahn School of Medicine at Mount Sinai, where PacBio sequencing libraries were prepared and sequenced. JMU performed all short- and long-read assemblies, genome polishing, assembly evaluations, repeat modeling and annotation, and gene annotation. JMU did all RNA work and library preparations for all RNA-seq samples representing replicates from both sexes at different stages, and performed all transcriptome assemblies and RNA-seq data analysis. JMU performed DNA modification analyses with PacBio single molecule kinetics data and MinION single molecule ionic current data. CMC made DNA plugs from *Sciara* pupae collected and sent to her by JMU, and performed the BioNano preparations and imaging on Irys platform. RM and NL performed BioNano hybrid scaffolding with selected assemblies sent to them. SJB provided guidance in our acquisition of BioNano data and provided oversight to CMC, RM, and NL. MSF prepared the Illumina DNA library. JEB did all *Sciara* mass matings. ACS provided support and guidance on this work. SAG pioneered and guided the *Sciara* genome effort. JMU conceived the experiments and analyses. JMU and SAG wrote the manuscript.

REFERENCES

Altschul SF, Gish W, Miller W, Myers EW, Lipman DJ. 1990. Basic local alignment search tool. *J Mol Biol* **215**: 403–410.

Andersson SGE, Zomorodipour A, Andersson JO, Sicheritz-Pontén T, Alsmark UCM, Podowski RM, Näslund AK, Eriksson A-S, Winkler HH, Kurland CG. 1998. The genome sequence of Rickettsia prowazekii and the origin of mitochondria. *Nature* **396**: 133–140.

Armstrong MJ, Jin Y, Allen EG, Jin P. 2019. Diverse and dynamic DNA modifications in brain and diseases. *Hum Mol Genet* **28**: R241–R253.

Bailey TL, Elkan C. 1994. Fitting a mixture model by expectation maximization to discover motifs in biopolymers. *Proc Int Conf Intell Syst Mol Biol* **2**: 28–36.

Bankevich A, Nurk S, Antipov D, Gurevich AA, Dvorkin M, Kulikov AS, Lesin VM, Nikolenko SI, Pham S, Prjibelski AD, et al. 2012. SPAdes: A New Genome Assembly Algorithm and Its Applications to Single-Cell Sequencing. *J Comput Biol* **19**: 455–477.

Bao W, Kojima KK, Kohany O. 2015. Repbase Update, a database of repetitive elements in eukaryotic genomes. *Mob DNA* **6**: 11.

Bewick AJ, Vogel KJ, Moore AJ, Schmitz RJ. 2017. Evolution of DNA methylation across insects. *Mol Biol Evol* **34**: 654–665.

Bienz-Tadmor B, Smith HS, Gerbi SA. 1991. The promoter of DNA puff gene II/9-1 of Sciara coprophila is inducible by ecdysone in late prepupal salivary glands of Drosophila melanogaster. *Cell Regul* **2**: 875–88.

Bird AP. 1980. DNA methylation and the frequency of CpG in animal DNA. *Nucleic Acids Res* **8**: 1499–1504.

Blackmon H, Ross L, Bachtrog D. 2017. Sex determination, sex chromosomes, and karyotype evolution in insects. In *Journal of Heredity*, Vol. 108 of, pp. 78–93, Oxford University Press.

Boivin A, Vendrely R, C Vendrely. 1948. L'acide désoxyribonucléique du noyau cellulaire, dépositaire des caractères héréditaires; arguments d'ordre analytique. *Comp trend Acad Sci* **226**: 1061–1063.

Bolger AM, Lohse M, Usadel B. 2014. Trimmomatic: a flexible trimmer for Illumina sequence data. *Bioinformatics* **30**: 2114–20.

Capuano F, Mülleder M, Kok R, Blom HJ, Ralser M. 2014. Cytosine DNA Methylation Is Found in Drosophila melanogaster but Absent in Saccharomyces cerevisiae, Schizosaccharomyces pombe, and Other Yeast Species. *Anal Chem* **86**: 3697–3702.

Chaisson MJ, Tesler G. 2012. Mapping single molecule sequencing reads using basic local alignment with successive refinement (BLASR): application and theory. *BMC Bioinformatics* **13**: 238.

Chin C-S, Alexander DH, Marks P, Klammer AA, Drake J, Heiner C, Clum A, Copeland A, Huddleston J, Eichler EE, et al. 2013. Nonhybrid, finished microbial genome assemblies from long-read SMRT sequencing data. *Nat Methods* **10**: 563–9.

Chin C-S, Peluso P, Sedlazeck FJ, Nattestad M, Concepcion GT, Clum A, Dunn C, O'Malley R, Figueroa-Balderas R, Morales-Cruz A, et al. 2016. Phased diploid genome assembly with single-molecule real-time sequencing. *Nat Methods*.

Chodavarapu RK, Feng S, Bernatavichute Y V., Chen PY, Stroud H, Yu Y, Hetzel JA, Kuo F, Kim J, Cokus SJ, et al. 2010. Relationship between nucleosome positioning and DNA methylation.

Nature **466**: 388–392.
Clark ME, Anderson CL, Cande J, Karr TL. 2005. Widespread prevalence of Wolbachia in laboratory stocks and the implications for Drosophila research. *Genetics* **170**: 1667–1675.
Clark SC, Egan R, Frazier PI, Wang Z. 2013. ALE: a generic assembly likelihood evaluation framework for assessing the accuracy of genome and metagenome assemblies. *Bioinformatics* **29**: 435–43.
Clark TA, Murray IA, Morgan RD, Kislyuk AO, Spittle KE, Boitano M, Fomenkov A, Roberts RJ, Korlach J. 2012. Characterization of DNA methyltransferase specificities using single-molecule, real-time DNA sequencing. *Nucleic Acids Res* **40**: e29.
Collings CK, Anderson JN. 2017. Links between DNA methylation and nucleosome occupancy in the human genome. *Epigenetics and Chromatin* **10**.
Crooks GE, Hon G, Chandonia J-M, Brenner SE. 2004. WebLogo: a sequence logo generator. *Genome Res* **14**: 1188–90.
Crouse HV, Brown A, Mumford BC. 1971. L-chromosome inheritance and the problem of chromosome "imprinting" in Sciara (Sciaridae, Diptera). *Chromosoma* **34**: 324–339.
Crouse H V., Gerbi SA, Liang CM, Magnus L, Mercer IM. 1977. Localization of ribosomal DNA within the proximal X heterochromatin of Sciara coprophila (Diptera, Sciaridae). *Chromosoma* **64**: 305–318.
Crouse H V. 1960. The Controlling Element in Sex Chromosome Behavior in Sciara. *Genetics* **45**: 1429–43.
de Saint Phalle B, Sullivan W. 1996. Incomplete sister chromatid separation is the mechanism of programmed chromosome elimination during early Sciara coprophila embryogenesis. *Development* **122**: 3775–84.
de Saint Phalle B, Sullivan W. 1998. Spindle assembly and mitosis without centrosomes in parthenogenetic Sciara embryos. *J Cell Biol* **141**: 1383–91.
Deshmukh S, Ponnaluri VKC, Dai N, Pradhan S, Deobagkar D. 2018. Levels of DNA cytosine methylation in the Drosophila genome. *PeerJ* **2018**.
DiBartolomeis SM, Gerbi SA. 1989. Molecular characterization of DNA puff II/9A genes in Sciara coprophila. *J Mol Biol* **210**: 531–40.
Eastman EM, Goodman RM, Erlanger BF, Miller OJ. 1980. 5-Methylcytosine in the DNA of the polytene chromosomes of the dipteraSciara coprophila,Drosophila melanogaster andD. persimilis. *Chromosoma* **79**: 225–239.
Eid J, Fehr A, Gray J, Luong K, Lyle J, Otto G, Peluso P, Rank D, Baybayan P, Bettman B, et al. 2009. Real-Time DNA Sequencing from Single Polymerase Molecules. *Science (80-)* **323**.
El-Gebali S, Mistry J, Bateman A, Eddy SR, Luciani A, Potter SC, Qureshi M, Richardson LJ, Salazar GA, Smart A, et al. 2019. The Pfam protein families database in 2019. *Nucleic Acids Res* **47**: D427–D432.
English AC, Richards S, Han Y, Wang M, Vee V, Qu J, Qin X, Muzny DM, Reid JG, Worley KC, et al. 2012. Mind the gap: upgrading genomes with Pacific Biosciences RS long-read sequencing technology. *PLoS One* **7**: e47768.
Escribá MC, Greciano PG, Méndez-Lago M, De Pablos B, Trifonov VA, Ferguson-Smith MA, Goday C, Villasante A. 2011. Molecular and cytological characterization of repetitive DNA sequences from the centromeric heterochromatin of Sciara coprophila. *Chromosoma* **120**: 387–397.

Felsheim RF, Kurtti TJ, Munderloh UG. 2009. Genome Sequence of the Endosymbiont Rickettsia peacockii and Comparison with Virulent Rickettsia rickettsii: Identification of Virulence Factors ed. N. Ahmed. *PLoS One* **4**: e8361.

Flusberg BA, Webster DR, Lee JH, Travers KJ, Olivares EC, Clark TA, Korlach J, Turner SW. 2010. Direct detection of DNA methylation during single-molecule, real-time sequencing. *Nat Methods* **7**: 461–465.

Foulk MS, Liang C, Wu N, Blitzblau HG, Smith H, Alam D, Batra M, Gerbi SA. 2006. Ecdysone induces transcription and amplification in Sciara coprophila DNA puff II/9A. *Dev Biol* **299**: 151–63.

Foulk MS, Waggener JM, Johnson JM, Yamamoto Y, Liew GM, Urnov FD, Young Y, Lee G, Smith HS, Gerbi SA. 2013. Isolation and characterization of the ecdysone receptor and its heterodimeric partner ultraspiracle through development in Sciara coprophila. *Chromosoma* **122**: 103–19.

Fu Y, Luo G-Z, Chen K, Deng X, Yu M, Han D, Hao Z, Liu J, Lu X, Doré LC, et al. 2015. N6-Methyldeoxyadenosine Marks Active Transcription Start Sites in Chlamydomonas. *Cell* **161**: 879–892.

Gabrusewycz-Garcia N. 1964. Cytological and autoradiographic studies in Sciara coprophila salivary gland chromosomes. *Chromosoma* **15**: 312–44.

Gerbi SA. 1971. Localization and characterization of the ribosomal RNA cistrons in Sciara coprophila. *J Mol Biol* **58**: 499–511.

Gerbi SA. 1986. Unusual chromosome movements in sciarid flies. *Results Probl Cell Differ* **13**: 71–104.

Gerbi SA, Strezoska Z, Waggener JM. 2002. Initiation of DNA replication in multicellular eukaryotes. *J Struct Biol* **140**: 17–30.

Ghodsi M, Hill CM, Astrovskaya I, Lin H, Sommer DD, Koren S, Pop M. 2013. De novo likelihood-based measures for comparing genome assemblies. *BMC Res Notes* **6**: 334.

Goll MG, Bestor TH. 2005. Eukaryotic Cytosine Methyltransferases. *Annu Rev Biochem* **74**: 481–514.

Grabherr MG, Haas BJ, Yassour M, Levin JZ, Thompson DA, Amit I, Adiconis X, Fan L, Raychowdhury R, Zeng Q, et al. 2011. Full-length transcriptome assembly from RNA-Seq data without a reference genome. *Nat Biotechnol* **29**: 644–52.

Greciano PG, Ruiz MF, Kremer L, Goday C. 2009. Two new chromodomain-containing proteins that associate with heterochromatin in Sciara coprophila chromosomes. *Chromosoma* **118**: 361–376.

Greer EL, Blanco MA, Gu L, Sendinc E, Liu J, Aristizábal-Corrales D, Hsu C-H, Aravind L, He C, Shi Y. 2015. DNA Methylation on N6-Adenine in C. elegans. *Cell* **161**: 868–878.

Hennig W. 1973. Diptera (Two-winged Flies). *Handb Zool*.

Hoff KJ, Stanke M. 2019. Predicting Genes in Single Genomes with AUGUSTUS. *Curr Protoc Bioinforma* **65**: e57.

Holt C, Yandell M. 2011. MAKER2: an annotation pipeline and genome-database management tool for second-generation genome projects. *BMC Bioinformatics* **12**: 491.

Hubley R, Finn RD, Clements J, Eddy SR, Jones TA, Bao W, Smit AFA, Wheeler TJ. 2016. The Dfam database of repetitive DNA families. *Nucleic Acids Res* **44**: D81–D89.

Hunt M, Kikuchi T, Sanders M, Newbold C, Berriman M, Otto TD. 2013. REAPR: a universal tool

for genome assembly evaluation. *Genome Biol* **14**: R47.
Ip CLC, Loose M, Tyson JR, de Cesare M, Brown BL, Jain M, Leggett RM, Eccles DA, Zalunin V, Urban JM, et al. 2015. MinION Analysis and Reference Consortium: Phase 1 data release and analysis. *F1000Research* **4**.
Jia D, Jurkowska RZ, Zhang X, Jeltsch A, Cheng X. 2007. Structure of Dnmt3a bound to Dnmt3L suggests a model for de novo DNA methylation. *Nature* **449**: 248–251.
Kajitani R, Toshimoto K, Noguchi H, Toyoda A, Ogura Y, Okuno M, Yabana M, Harada M, Nagayasu E, Maruyama H, et al. 2014. Efficient de novo assembly of highly heterozygous genomes from whole-genome shotgun short reads. *Genome Res* **24**: 1384–95.
Kato Y, Kaneda M, Hata K, Kumaki K, Hisano M, Kohara Y, Okano M, Li E, Nozaki M, Sasaki H. 2007. Role of the Dnmt3 family in de novo methylation of imprinted and repetitive sequences during male germ cell development in the mouse. *Hum Mol Genet* **16**: 2272–2280.
Kerrebrock AW, Srivastava R, Gerbi SA. 1989. Isolation and characterization of ribosomal DNA variants from Sciara coprophila. *J Mol Biol* **210**: 1–13.
Kim D, Paggi JM, Park C, Bennett C, Salzberg SL. 2019. Graph-based genome alignment and genotyping with HISAT2 and HISAT-genotype. *Nat Biotechnol* **37**: 907–915.
Koren S, Walenz BP, Berlin K, Miller JR, Bergman NH, Phillippy AM. 2017. Canu: Scalable and accurate long-read assembly via adaptive κ-mer weighting and repeat separation. *Genome Res* **27**: 722–736.
Korf I. 2004. Gene finding in novel genomes. *BMC Bioinformatics* **5**: 59.
Laetsch DR, Blaxter ML. 2017. BlobTools: Interrogation of genome assemblies. *F1000Research* **6**: 1287.
Lam ET, Hastie A, Lin C, Ehrlich D, Das SK, Austin MD, Deshpande P, Cao H, Nagarajan N, Xiao M, et al. 2012. Genome mapping on nanochannel arrays for structural variation analysis and sequence assembly. *Nat Biotechnol* **30**: 771–776.
Langmead B, Salzberg SL. 2012. Fast gapped-read alignment with Bowtie 2. *Nat Methods* **9**: 357–9.
Lawson ET, Mousseau TA, Klaper R, Hunter MD, Werren JH. 2001. Rickettsia associated with male-killing in a buprestid beetle. *Heredity (Edinb)* **86**: 497–505.
Li B, Fillmore N, Bai Y, Collins M, Thomson JA, Stewart R, Dewey CN. 2014. Evaluation of de novo transcriptome assemblies from RNA-Seq data. *Genome Biol* **15**: 553.
Li D, Liu C-M, Luo R, Sadakane K, Lam T-W. 2015. MEGAHIT: an ultra-fast single-node solution for large and complex metagenomics assembly via succinct de Bruijn graph. *Bioinformatics* **31**: 1674–1676.
Li E, Beard C, Jaenisch R. 1993. Role for DNA methylation in genomic imprinting. *Nature* **366**: 362–5.
Li H. 2016. Minimap and miniasm: fast mapping and de novo assembly for noisy long sequences. *Bioinformatics* **32**: 2103–10.
Li H. 2018. Minimap2: Pairwise alignment for nucleotide sequences. *Bioinformatics* **34**: 3094–3100.
Li H, Durbin R. 2009. Fast and accurate short read alignment with Burrows-Wheeler transform. *Bioinformatics* **25**: 1754–60.
Lin Y, Yuan J, Kolmogorov M, Shen MW, Chaisson M, Pevzner PA. 2016. Assembly of long error-

prone reads using de Bruijn graphs. *Proc Natl Acad Sci U S A* **113**: E8396–E8405.

Liu J, Zhu Y, Luo G-Z, Wang X, Yue Y, Wang X, Zong X, Chen K, Yin H, Fu Y, et al. 2016. Abundant DNA 6mA methylation during early embryogenesis of zebrafish and pig. *Nat Commun* **7**: 13052.

Loman NJ, Quick J, Simpson JT. 2015. A complete bacterial genome assembled de novo using only nanopore sequencing data. *Nat Methods* **advance on**.

Luo G-Z, Blanco MA, Greer EL, He C, Shi Y. 2015. DNA N(6)-methyladenine: a new epigenetic mark in eukaryotes? *Nat Rev Mol Cell Biol* **16**: 705–10.

Luo G-Z, Hao Z, Luo L, Shen M, Sparvoli D, Zheng Y, Zhang Z, Weng X, Chen K, Cui Q, et al. 2018. N6-methyldeoxyadenosine directs nucleosome positioning in Tetrahymena DNA. *Genome Biol* **19**: 200.

Luo R, Liu B, Xie Y, Li Z, Huang W, Yuan J, He G, Chen Y, Pan Q, Liu Y, et al. 2012. SOAPdenovo2: an empirically improved memory-efficient short-read de novo assembler. *Gigascience* **1**: 18.

Matthews BJ, Dudchenko O, Kingan SB, Koren S, Antoshechkin I, Crawford JE, Glassford WJ, Herre M, Redmond SN, Rose NH, et al. 2018. Improved reference genome of Aedes aegypti informs arbovirus vector control. *Nature* **563**: 501–507.

Mavrich TN, Jiang C, Ioshikhes IP, Li X, Venters BJ, Zanton SJ, Tomsho LP, Qi J, Glaser RL, Schuster SC, et al. 2008. Nucleosome organization in the Drosophila genome. *Nature* **453**: 358–362.

McAlpine JF, Wood DM. 1989. Manual of Nearctic Diptera. *Agric Canada Monogr* **3**.

Mendelowitz LM, Schwartz DC, Pop M. 2015. Maligner: a fast ordered restriction map aligner. *Bioinformatics* **32**: 1016–1022.

Mok EH, Smith HS, DiBartolomeis SM, Kerrebrock AW, Rothschild LJ, Lange TS, Gerbi SA. 2001. Maintenance of the DNA puff expanded state is independent of active replication and transcription. *Chromosoma* **110**: 186–96.

Mondo SJ, Dannebaum RO, Kuo RC, Louie KB, Bewick AJ, LaButti K, Haridas S, Kuo A, Salamov A, Ahrendt SR, et al. 2017. Widespread adenine N6-methylation of active genes in fungi. *Nat Genet* **49**: 964–968.

Nigro RG, Campos MCC, Perondini ALP. 2007. Temperature and the progeny sex-ratio in Sciara ocellaris (Diptera, Sciaridae). *Genet Mol Biol* **30**: 152–158.

Nikolenko SI, Korobeynikov AI, Alekseyev MA. 2013. BayesHammer: Bayesian clustering for error correction in single-cell sequencing. *BMC Genomics* **14 Suppl 1**: S7.

Panikar CS, Rajpathak SN, Abhyankar V, Deshmukh S, Deobagkar DD. 2015. Presence of DNA methyltransferase activity and CpC methylation in Drosophila melanogaster. *Mol Biol Rep* **42**: 1615–1621.

Pardue M Lou, Gerbi SA, Eckhardt RA, Gall JG. 1970. Cytological localization of DNA complementary to ribosomal RNA in polytene chromosomes of Diptera. *Chromosoma* **29**: 268–290.

Patro R, Duggal G, Love MI, Irizarry RA, Kingsford C. 2017. Salmon provides accurate, fast, and bias-aware transcript expression. *Nat Methods* **14**: 417–419.

Pertea M, Pertea GM, Antonescu CM, Chang TC, Mendell JT, Salzberg SL. 2015. StringTie enables improved reconstruction of a transcriptome from RNA-seq reads. *Nat Biotechnol* **33**: 290–295.

Quevillon E, Silventoinen V, Pillai S, Harte N, Mulder N, Apweiler R, Lopez R. 2005. InterProScan: protein domains identifier. *Nucleic Acids Res* **33**: W116-20.

Quinlan AR, Hall IM. 2010. BEDTools: a flexible suite of utilities for comparing genomic features. *Bioinformatics* **26**: 841–2.

Raddatz G, Guzzardo PM, Olova N, Fantappié MR, Rampp M, Schaefer M, Reik W, Hannon GJ, Lyko F. 2013. Dnmt2-dependent methylomes lack defined DNA methylation patterns. *Proc Natl Acad Sci U S A* **110**: 8627–8631.

Rasch EM. 1970b. DNA cytophotometry of salivary gland nuclei and other tissue systems in dipteran larvae. In *In Introduction to Quantitative Cytochemistry* (eds. G.L. Wied and G.F. Bahr), pp. 357–397, Academic Press, New York.

Rasch EM. 2006. Genome size and determination of DNA content of the X chromosomes, autosomes, and germ line-limited chromosomes of Sciara coprophila. *J Morphol* **267**: 1316–25.

Rasch EM. 1970a. Two-wavelength cytophotometry of Sciara salivary gland chromosomes. In *Introduction to Quantitative Cytochemistry* (eds. G.L. Wied and G.F. Bahr), Vol. 2 of, pp. 335–355, Academic Press, New York.

Rausch C, Hastert FD, Cardoso MC. 2020. DNA Modification Readers and Writers and Their Interplay. *J Mol Biol*.

Roach MJ, Schmidt SA, Borneman AR. 2018. Purge Haplotigs: allelic contig reassignment for third-gen diploid genome assemblies. *BMC Bioinformatics* **19**: 460.

Salzberg SL, Phillippy AM, Zimin A, Puiu D, Magoc T, Koren S, Treangen TJ, Schatz MC, Delcher AL, Roberts M, et al. 2012. GAGE: A critical evaluation of genome assemblies and assembly algorithms. *Genome Res* **22**: 557–67.

Sedlazeck FJ, Rescheneder P, Smolka M, Fang H, Nattestad M, von Haeseler A, Schatz MC. 2018. Accurate detection of complex structural variations using single-molecule sequencing. *Nat Methods* **15**: 461–468.

Serbus LR, Casper-Lindley C, Landmann F, Sullivan W. 2008. The Genetics and Cell Biology of *Wolbachia* -Host Interactions. *Annu Rev Genet* **42**: 683–707.

Sformo T, Kohl F, McIntyre J, Kerr P, Duman JG, Barnes BM. 2009. Simultaneous freeze tolerance and avoidance in individual fungus gnats, Exechia nugatoria. *J Comp Physiol B Biochem Syst Environ Physiol* **179**: 897–902.

Sharakhova M V., Hammond MP, Lobo NF, Krzywinski J, Unger MF, Hillenmeyer ME, Bruggner R V., Birney E, Collins FH. 2007. Update of the Anopheles gambiae pest genome assembly. *Genome Biol* **8**.

Simão FA, Waterhouse RM, Ioannidis P, Kriventseva E V, Zdobnov EM. 2015. BUSCO: assessing genome assembly and annotation completeness with single-copy orthologs. *Bioinformatics* **31**.

Simpson JT, Durbin R. 2010. Efficient construction of an assembly string graph using the FM-index. *Bioinformatics* **26**: i367-73.

Simpson JT, Wong K, Jackman SD, Schein JE, Jones SJM, Birol I. 2009. ABySS: a parallel assembler for short read sequence data. *Genome Res* **19**: 1117–23.

Simpson JT, Workman RE, Zuzarte PC, David M, Dursi LJ, Timp W. 2017. Detecting DNA cytosine methylation using nanopore sequencing. *Nat Methods* **14**: 407–410.

Smit A, Hubley R. 2008. RepeatModeler Open-1.0. http://www.repeatmasker.org.

1409 Smit A, Hubley R, Green P. 2013. RepeatMasker Open-4.0. http://www.repeatmasker.org.
1410 Smith-Unna R, Boursnell C, Patro R, Hibberd JM, Kelly S. 2016. TransRate: reference-free quality
1411 assessment of de novo transcriptome assemblies. *Genome Res* **26**: 1134–44.
1412 Stuart JJ, Chen M-S, Shukle R, Harris MO. 2012. Gall Midges (Hessian Flies) as Plant Pathogens.
1413 *Annu Rev Phytopathol* **50**: 339–357.
1414 Suzuki Y, Korlach J, Turner SW, Tsukahara T, Taniguchi J, Qu W, Ichikawa K, Yoshimura J, Yurino
1415 H, Takahashi Y, et al. 2016. AgIn: measuring the landscape of CpG methylation of individual
1416 repetitive elements. *Bioinformatics* **32**: 2911–9.
1417 Takayama S, Dhahbi J, Roberts A, Mao G, Heo S-J, Pachter L, Martin DIK, Boffelli D. 2014.
1418 Genome methylation in D. melanogaster is found at specific short motifs and is
1419 independent of DNMT2 activity. *Genome Res* **24**: 821–830.
1420 The UniProt Consortium. 2019. UniProt: A worldwide hub of protein knowledge. *Nucleic Acids*
1421 *Res* **47**: D506–D515.
1422 Ter-Hovhannisyan V, Lomsadze A, Chernoff YO, Borodovsky M. 2008. Gene prediction in novel
1423 fungal genomes using an ab initio algorithm with unsupervised training. *Genome Res* **18**:
1424 1979–90.
1425 Urban JM, Bliss J, Lawrence CE, Gerbi SA. 2015. Sequencing ultra-long DNA molecules with the
1426 Oxford Nanopore MinION. *bioRxiv* doi: 10.1101/019281.
1427 Urnov FD, Liang C, Blitzblau HG, Smith HS, Gerbi SA. 2002. A DNase I hypersensitive site flanks
1428 an origin of DNA replication and amplification in Sciara. *Chromosoma* **111**: 291–303.
1429 Vaser R, Sović I, Nagarajan N, Šikić M. 2017. Fast and accurate de novo genome assembly from
1430 long uncorrected reads. *Genome Res* **27**: 737–746.
1431 Vezzi F, Narzisi G, Mishra B, Nagarajan N, Pop M, Vezzi F, Narzisi G, Mishra B, Lander E, Linton L,
1432 et al. 2012. Reevaluating Assembly Evaluations with Feature Response Curves: GAGE and
1433 Assemblathons ed. A. Rzhetsky. *PLoS One* **7**: e52210.
1434 Walker BJ, Abeel T, Shea T, Priest M, Abouelliel A, Sakthikumar S, Cuomo CA, Zeng Q, Wortman
1435 J, Young SK, et al. 2014. Pilon: an integrated tool for comprehensive microbial variant
1436 detection and genome assembly improvement. *PLoS One* **9**: e112963.
1437 Wang X, Li Z, Zhang Q, Li B, Lu C, Li W, Cheng T, Xia Q, Zhao P. 2018. DNA methylation on N6-
1438 adenine in lepidopteran Bombyx mori. *Biochim Biophys Acta - Gene Regul Mech* **1861**:
1439 815–825.
1440 Wang Y, Chen X, Sheng Y, Liu Y, Gao S. 2017. N6-adenine DNA methylation is associated with
1441 the linker DNA of H2A.Z-containing well-positioned nucleosomes in Pol II-transcribed
1442 genes in Tetrahymena. *Nucleic Acids Res* **45**: 11594–11606.
1443 Werren JH, Windsor DM. 2000. Wolbachia infection frequencies in insects: Evidence of a global
1444 equilibrium? *Proc R Soc B Biol Sci* **267**: 1277–1285.
1445 White MJ. 1949. Cytological evidence on the phylogeny and classification of the Diptera.
1446 *Evolution* **3**: 252–261.
1447 Wiegmann BM, Richards S. 2018. Genomes of Diptera. *Curr Opin Insect Sci* **25**: 116–124.
1448 Wiegmann BM, Trautwein MD, Winkler IS, Barr NB, Kim JW, Lambkin C, Bertone MA, Cassel BK,
1449 Bayless KM, Heimberg AM, et al. 2011. Episodic radiations in the fly tree of life. *Proc Natl*
1450 *Acad Sci U S A* **108**: 5690–5695.
1451 Wu N, Liang C, DiBartolomeis SM, Smith HS, Gerbi SA. 1993. Developmental progression of DNA
1452 puffs in Sciara coprophila: amplification and transcription. *Dev Biol* **160**: 73–84.

1453 Xiao C-L, Zhu S, He M, Chen D, Zhang Q, Chen Y, Yu G, Liu J, Xie S-Q, Luo F, et al. 2018. N6-
1454 Methyladenine DNA Modification in the Human Genome. *Mol Cell* **71**: 306-318.e7.
1455 Ye C, Hill CM, Wu S, Ruan J, Ma Z (Sam). 2016. DBG2OLC: Efficient Assembly of Large Genomes
1456 Using Long Erroneous Reads of the Third Generation Sequencing Technologies. *Sci Rep* **6**:
1457 31900.
1458 Zemach A, McDaniel IE, Silva P, Zilberman D. 2010. Genome-wide evolutionary analysis of
1459 eukaryotic DNA methylation. *Science (80-)* **328**: 916–919.
1460 Zerbino DR, Birney E. 2008. Velvet: algorithms for de novo short read assembly using de Bruijn
1461 graphs. *Genome Res* **18**: 821–9.
1462 Zhang G, Huang H, Liu D, Cheng Y, Liu X, Zhang W, Yin R, Zhang D, Zhang P, Liu J, et al. 2015. N6-
1463 Methyladenine DNA Modification in Drosophila. *Cell* **161**: 893–906.
1464 Zhou C, Wang C, Liu H, Zhou Q, Liu Q, Guo Y, Peng T, Song J, Zhang J, Chen L, et al. 2018.
1465 Identification and analysis of adenine N6-methylation sites in the rice genome. *Nat Plants*
1466 **4**: 554–563.
1467